Article

Cell Reports

Identification of Metabolically Distinct Adipocyte Progenitor Cells in Human Adipose Tissues

Graphical Abstract

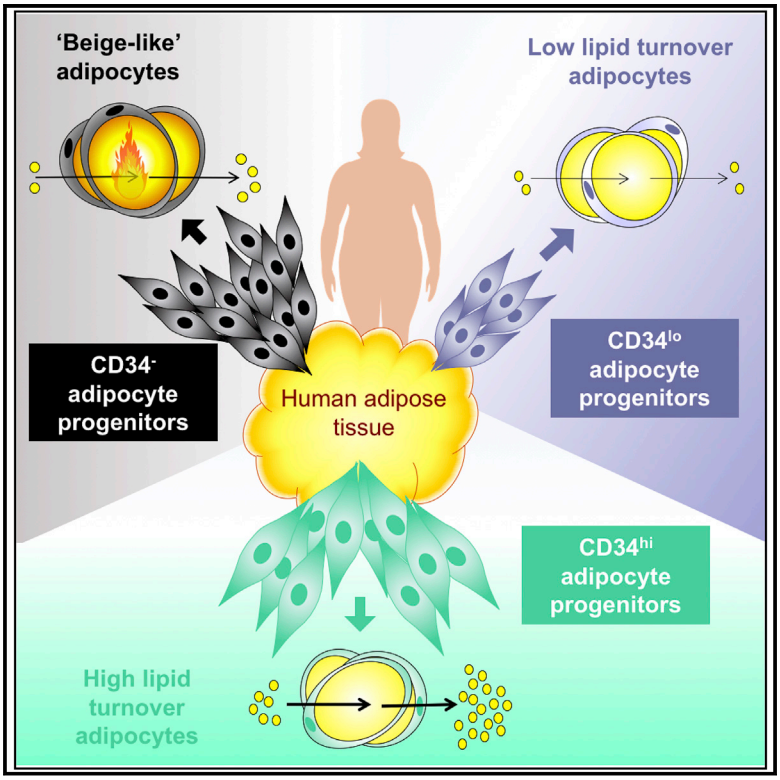

Authors

Arthe Raajendiran, Geraldine Ooi, Jackie Bayliss, ..., Matthew S. Rodeheffer, Paul R. Burton, Matthew J. Watt

Correspondence

matt.watt@unimelb.edu.au

In Brief

Raajendiran et al. report the identification of three adipocyte progenitor cell (APC) subtypes that reside in human adipose tissues. These APCs have distinct molecular phenotypes yet retain similar adipogenic potential. The APCs give rise to adipocytes with divergent metabolic and endocrine capacities and their distribution varies in type 2 diabetes patients.

Highlights

- Identification of three distinct human adipocyte progenitor cell (APC) subtypes
- APC subtypes have unique molecular profiles but similar adipogenic capacities
- Adipocytes from APC subtypes have distinguishing metabolic and endocrine profiles
- APC composition varies according to anatomical location and type 2 diabetes status

Raajendiran et al., 2019, Cell Reports *27*, 1528–1540
April 30, 2019
https://doi.org/10.1016/j.celrep.2019.04.010

CellPress

OPEN ACCESS
CellPress

Cell Reports
Article

Identification of Metabolically Distinct Adipocyte Progenitor Cells in Human Adipose Tissues

Arthe Raajendiran,[1,2,3] Geraldine Ooi,[6] Jackie Bayliss,[1] Paul E. O'Brien,[6] Ralf B. Schittenhelm,[7] Ashlee K. Clark,[4,5] Renea A. Taylor,[2,4] Matthew S. Rodeheffer,[8] Paul R. Burton,[6] and Matthew J. Watt[1,2,3,9,*]

[1]Department of Physiology, The University of Melbourne, Melbourne, VIC 3010, Australia
[2]Department of Physiology, Monash University, Clayton, VIC 3800, Australia
[3]Metabolism, Diabetes and Obesity Program, Monash Biomedicine Discovery Institute, Monash University, Clayton, VIC 3800, Australia
[4]Cancer Program, Monash Biomedicine Discovery Institute, Monash University, Clayton, VIC 3800, Australia
[5]Department of Anatomy and Developmental Biology, Monash University, Clayton, VIC 3800, Australia
[6]Centre for Obesity Research and Education, Faculty of Medicine, Nursing and Health Sciences, Monash University, Melbourne, VIC 3004, Australia
[7]Monash Biomedical Proteomics Facility and Department of Biochemistry and Molecular Biology, Wellington Road, Monash University, Clayton, VIC 3800, Australia
[8]Department of Molecular Cell and Developmental Biology; Program in Integrative Cell Signaling and Neurobiology of Metabolism, Department of Comparative Medicine; and Yale Stem Cell Center, Yale University, New Haven, CT, USA
[9]Lead Contact
*Correspondence: matt.watt@unimelb.edu.au
https://doi.org/10.1016/j.celrep.2019.04.010

SUMMARY

Adipocyte progenitor cells (APCs) provide the reservoir of regenerative cells to produce new adipocytes, although their identity in humans remains elusive. Using FACS analysis, gene expression profiling, and metabolic and proteomic analyses, we identified three APC subtypes in human white adipose tissues. The APC subtypes are molecularly distinct but possess similar proliferative and adipogenic capacities. Adipocytes derived from APCs with high CD34 expression exhibit exceedingly high rates of lipid flux compared with APCs with low or no CD34 expression, while adipocytes produced from CD34$^-$ APCs display beige-like adipocyte properties and a unique endocrine profile. APCs were more abundant in gluteofemoral compared with abdominal subcutaneous and omental adipose tissues, and the distribution of APC subtypes varies between depots and in patients with type 2 diabetes. These findings provide a mechanistic explanation for the heterogeneity of human white adipose tissue and a potential basis for dysregulated adipocyte function in type 2 diabetes.

INTRODUCTION

The major function of adipose tissue is to maintain systemic energy balance through the storage and release of free fatty acids and via the secretion of adipokines, which communicate locally and with other organs to regulate food intake, energy expenditure, and a myriad of metabolic processes (Rosen and Spiegelman, 2014). Obesity and defective adipose tissue function is inextricably linked to the development of metabolic diseases, such as dyslipidemia and type 2 diabetes. In light of the continued increase in global obesity prevalence (Afshin et al., 2017), there remains intense interest in understanding how adipocytes develop and in unraveling the mechanisms that control metabolic and endocrine functions, especially in the face of overnutrition.

Adipose tissue expansion is driven by both hypertrophy and hyperplasia of adipocytes. Mature adipocytes are post-mitotic, and ~8% of adipocytes are turned over each year to match the rates of cell death (Spalding et al., 2008). New adipocytes are derived from the proliferation and differentiation of preadipocytes or adipocyte progenitor cells (APCs), which reside within the stromal vascular fraction of adipose tissue. While the precise origin of the APCs is unresolved (Berry et al., 2014b), prospective approaches have established CD31$^-$, CD45$^-$, CD29$^+$, CD34$^+$, Sca-1$^+$, and CD24$^+$ (or CD24$^-$) cells as committed murine white adipocyte progenitors capable of adipogenesis (Berry and Rodeheffer, 2013; Macotela et al., 2012; Rodeheffer et al., 2008). Transplantation of these cells into the primordial fat cavity of lipodystrophic mice formed a viable white adipose tissue depot and rescued the diabetic phenotype of these mice (Rodeheffer et al., 2008). In humans, several cell surface proteins are commonly reported to be expressed on stromal vascular fraction cells that can undergo adipogenesis (e.g., CD34, CD29, CD13, CD44, CD73, CD90, CD142, and CD9); however, there is no consensus on the molecular, metabolic, and endocrine profiles of adipocytes derived from specific human APC populations (Cawthorn et al., 2012).

Developmentally and functionally distinct adipocytes reside mixed together in the same adipose tissue depot (Chau et al., 2014; Ussar et al., 2014; Xue et al., 2015). At a molecular level, there is evidence of intrinsic heterogeneity in gene expression between mature adipocytes from the same fat depot (Blüher et al., 2004), and functionally, there is evidence of two distinct

triglyceride pools within adipose tissue that have low and high turnover rates (Ekstedt and Olivecrona, 1970; Stein and Stein, 1961). In supporting the concept of APC heterogeneity, recent studies employing RNA sequencing (RNA-seq) of single cells within the stromal vascular fraction of mouse white adipose tissues identified several major subsets of APCs that differed in their trajectories toward adipogenic differentiation (Burl et al., 2018; Schwalie et al., 2018). While one report indicates that human APCs are a single homogeneous cell population (Acosta et al., 2017), others have identified APC subtypes with distinct cell-dynamic properties in human adipose tissues (Gao et al., 2017; Tchkonia et al., 2005), raising the intriguing possibility that different populations of APCs co-exist in the same white adipose tissue depot of humans and give rise to adipocytes with varied metabolic and endocrine capacities.

The regional distribution of adipose tissue varies considerably, even among individuals with similar total body fat, and the clinical significance of body fat distribution is supported by epidemiological data showing a detrimental effect of visceral and upper body subcutaneous adipose tissues on cardiovascular and diabetes risk and a protective role for lower body gluteofemoral adipose tissue (Wajchenberg, 2000). Adipocytes isolated from different adipose tissue depots vary in their molecular phenotypes, size, responses to insulin and β-adrenergic agonists, in their capacity for lipolysis and fatty acid uptake, and in their production of secreted proteins (Arner, 2005; Raajendiran et al., 2016; Rantalainen et al., 2011; Rosen and Spiegelman, 2014; Tchkonia et al., 2013). While factors such as blood flow, innervation, and immune cell infiltration are likely to contribute to the regional differences in adipocyte functions (Rosen and Spiegelman, 2014; Tchkonia et al., 2013), the intrinsic characteristics of APCs within specific adipose tissue locations may influence the metabolic and endocrine properties of the terminally differentiated adipocytes.

In this study, we have identified three distinct human APC subtypes coexisting within the same adipose tissue depot. These APCs have similar adipogenic properties but are characterized by unique molecular profiles, and produce adipocytes with marked differences in their metabolic capacities and endocrine functions, and their potential for adaptive thermogenesis. We further show that the APC composition varies according to the anatomical location of the adipose tissue depots and that the distribution of APCs is altered in type 2 diabetes patients. These findings provide a mechanistic explanation for the heterogeneity of human white adipose tissue and a potential basis for dysregulated adipocyte function in type 2 diabetes.

RESULTS

Identification of APCs in Human Adipose Tissue

Murine cells expressing CD34, CD29, Sca1, and CD24 were previously identified as committed APCs (Rodeheffer et al., 2008; Berry and Rodeheffer, 2013). We used a similar fluorescence-activated cell sorting (FACS) approach to isolate putative human APCs from obese patients undergoing bariatric surgery procedures (Table S1). Adipose tissue was procured from the omentum (denoted as VAT), the abdominal subcutaneous region near the umbilicus (ASAT), and the subcutaneous gluteofemoral region (GFAT). Adipose tissue was digested, and cells of endothelial and hematopoietic linages within the stromal vascular fraction were depleted using the cell surface markers CD31 and CD45, respectively. The remaining cells were FACS sorted to identify likely APCs (Figures 1A–1C and S1A–S1G). Cell types within the stromal vascular fraction were identified based on CD marker expression profiles, and their distribution and clustering are shown in the *t*-distributed stochastic neighbor embedding 2D map (Figure 1B). Three distinct Lin^- $CD29^+$ APC populations were identified as APCs and collected based on their level of CD34 expression; these were named $CD34^{hi}$, $CD34^{lo}$, and $CD34^-$ APC subtypes (Figure 1C). Previous studies demonstrated that PDGFRα is expressed in the murine adipogenic cellular linage (Berry and Rodeheffer, 2013) and in white adipose tissue-resident cells that produce beige-like adipocytes (Lee et al., 2012). *PDGFRA* was expressed in all APC subtypes with the highest expression in $CD34^{hi}$, followed by $CD34^{lo}$ and $CD34^-$ (Table S2).

The $CD34^{hi}$ APCs were larger than $CD34^-$ and $CD34^{lo}$ APCs (Figure S2A), and their general morphology was dissimilar (Figure S2B). On average, the APCs constituted 37% of the total number of cells in the stromal vascular fraction of human adipose tissue (Figure S2C). APCs were most abundant in GFAT compared with ASAT and VAT, which had similar numbers of APCs (Figure 1D). The number of APCs were highly variable between individuals (Figures 1E–1G), and the degree of adiposity did not impact APC abundance (Figure S2D). The $CD34^-$ APCs were the most abundant, averaging 0.36×10^6 cells/g of adipose tissue, with half the number of $CD34^{hi}$ APCS (0.19×10^6 cells/g) and only 0.05×10^6 cells/g $CD34^{lo}$ APCs (Figure 1D). The number of APCs per gram of tissue was influenced by anatomical location. The $CD34^-$ APCs were significantly higher in GFAT when compared with both VAT and ASAT (Figure 1E), and the $CD34^{lo}$ APCs were most abundant in GFAT (Figure 1F). In contrast, there was significantly more $CD34^{hi}$ APCs in VAT when compared with ASAT, and $CD34^{hi}$ APCs tended to be higher in GFAT compared with ASAT (Figure 1G). Because adipocyte cell size is different between anatomical locations (Figure S2E; VAT < ASAT = GFAT) (Fang et al., 2015), we expressed the number of APCs relative to adipocyte number and draw the same conclusions as reported above (Figures S2F and S2G). In summary, these results demonstrate that APCs are most abundant in GFAT and similar in ASAT and VAT, that the subcutaneous depots (ASAT and GFAT) are highly enriched with $CD34^-$ followed by $CD34^{hi}$ and $CD34^{lo}$ APCs, while the intra-abdominal VAT depot has an equal number of $CD34^-$ and $CD34^{hi}$ APCs accompanied by a lower number of $CD34^{lo}$ APCs.

Recent studies reported the existence of so-called fibro-adipogenic progenitor cells that were denoted as $PDGFR\alpha^+$, $CD34^+$, and $CD44^+$ with high expression of $CD9^+$, and were characterized by increased fibrogenic potential in humans (Marcelin et al., 2017). Accordingly, we focused on the progenitor phenotype with emphasis on CD9 and fibrosis marker gene expression. Approximately, 35%–50% of the $CD34^-$ and $CD34^{hi}$ APCs expressed CD9, whereas CD9 was only expressed on ~5% of $CD34^{lo}$ APCs (Figure S2H). Examination of the flow cytograms did not show the presence of clearly defined CD9 high- or low-expressing cells in the APCs (Figure S2I). The previously

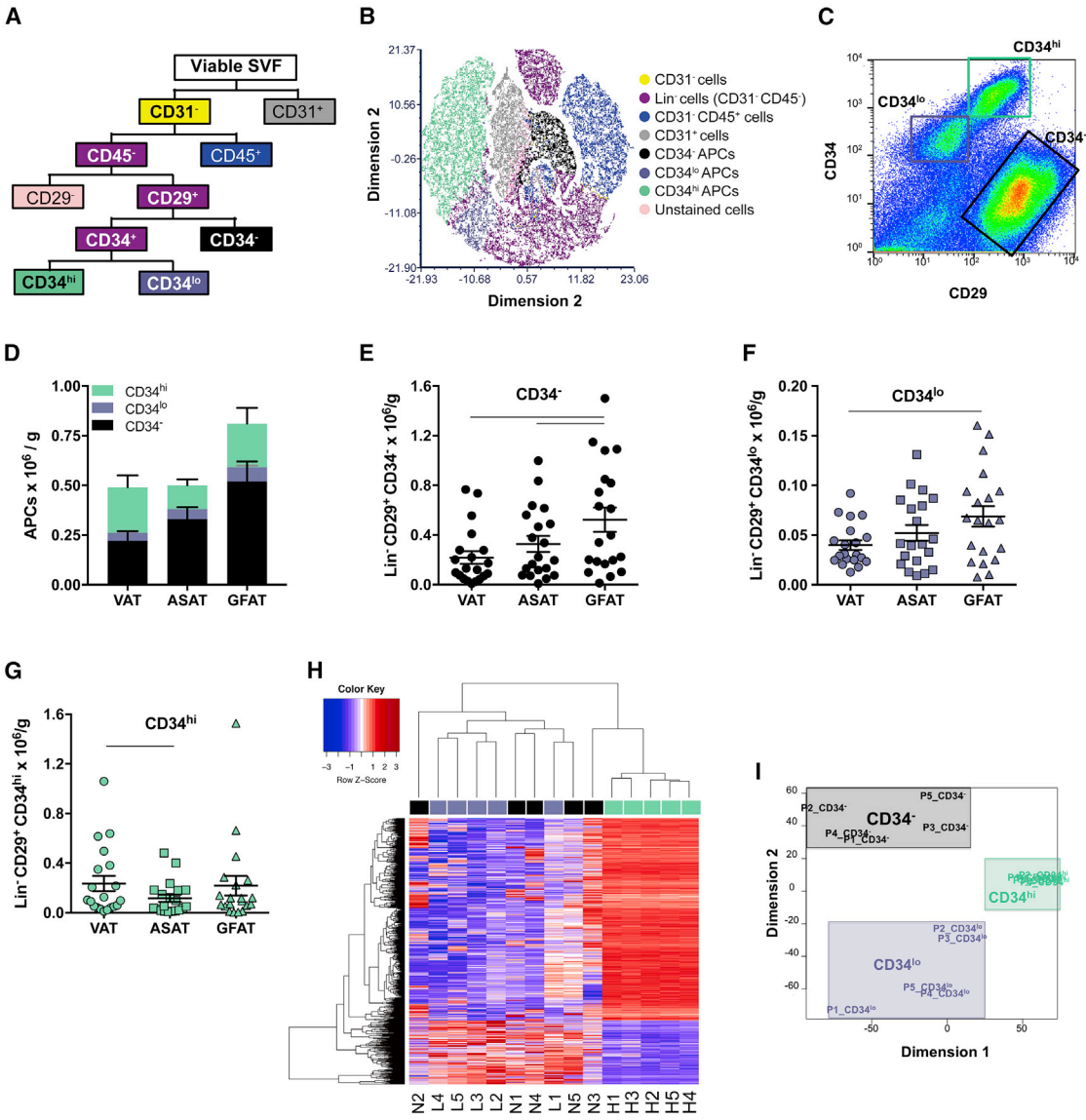

Figure 1. Identification of Human Adipocyte Progenitor Cells and Determination of Their Abundance by Anatomical Distribution

(A) FACS gating strategy for the identification of human APCs.

(B) t-Distributed Stochastic Neighbor Embedding 2D map (t-SNE plot) of 30,000 live stromal vascular fraction cells of abdominal subcutaneous adipose tissue. Plot shows the distribution of cell types based on their CD marker expression profiles. Populations within each plot are highlighted by colored boxes as per Figure 1A. The number of cells for each gated population is as follows: $CD31^-$ (25,794), Lin^- (20,204), $CD31^-$ $CD45^-$ (5,386), $CD31^+$ (3,569), $CD34^-$ (2,491), $CD34^{lo}$ (1,339), $CD34^{hi}$ (6,564), and unstained ($CD31^-$ $CD45^-$ $CD29^-$ $CD34^-$) (4,206).

(C) FACS plot showing CD34 and CD29 expression profiles of the individual APCs including Lin^- $CD29^+$ $CD34^-$ ($CD34^-$), Lin^- $CD29^+$ $CD34^{lo}$ ($CD34^{lo}$), and Lin^- $CD29^+$ $CD34^{hi}$ ($CD34^{hi}$) cells. Gated populations within each plot are highlighted by colored boxes as per Figure 1A.

(D) Histogram showing APC abundance in different adipose tissue depots. Data are means ± SEM for each APC subtype (n = 20).

(E–G) Number of APCs in different adipose tissue depots. $CD34^-$ (E), $CD34^{lo}$ (F), and $CD34^{hi}$ (G) APCs. Individual data points reported with the mean ± SEM (n = 20). Statistical significance was evaluated by one-way Friedman test with Dunn's multiple comparison using patient-matched data. $p < 0.05$ denoted by lines adjoining respective groups.

(H and I) Transcriptome analysis of freshly isolated APCs derived from VAT (n = 5 subjects).

(H) Heatmap and hierarchical clustering of RNA-seq analysis representing the differential expression of gene. H, $CD34^{hi}$; L, $CD34^{lo}$; N, $CD34^-$. Numbers after letters denote the patient number.

(I) Principal-component analysis highlighting the clustering of APC populations by subtype. P1–5 denote patient numbers. Black bordered box, $CD34^-$ APCs; purple bordered box, $CD34^{lo}$ APCs; green bordered box; $CD34^{hi}$ APCs.

See also Figure S1 and Tables S1, S2, and S3.

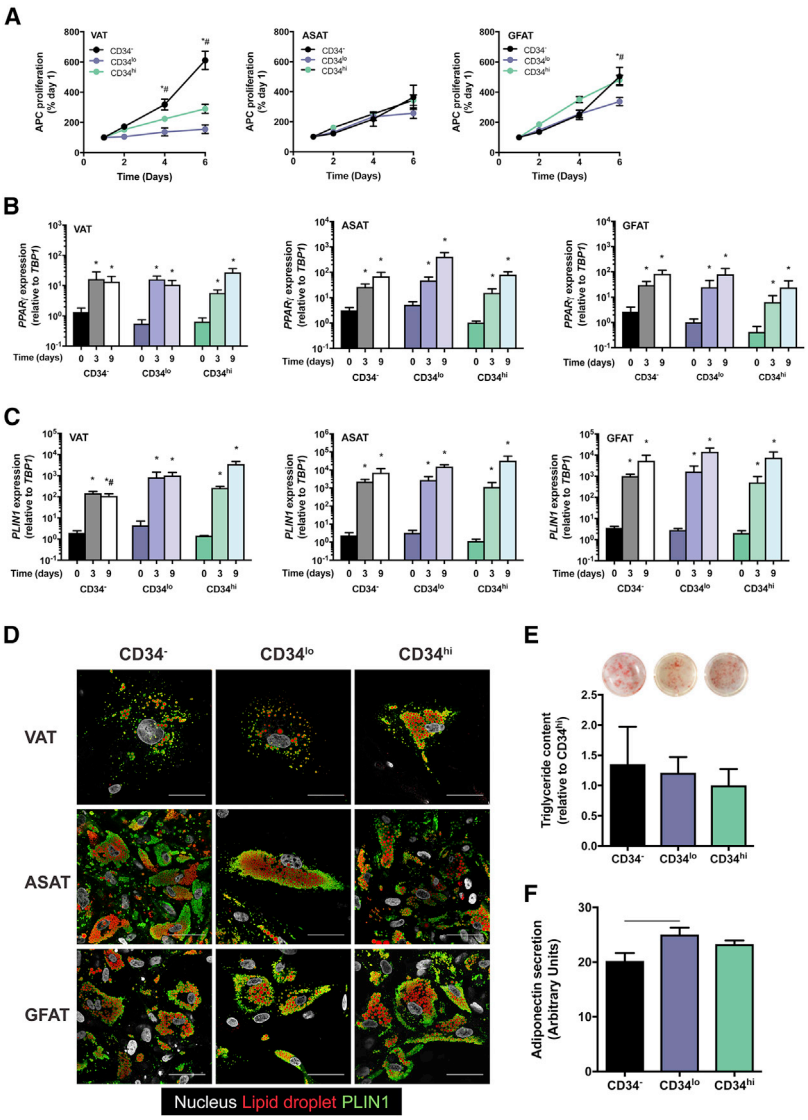

Figure 2. Human APC Subtypes Undergo Adipogenesis and Lipid Loading *In Vitro*

(A) Proliferation of APCs derived from VAT, ASAT, and GFAT (n = 5 patient-matched APC subtypes per depot; passage 2 cells). *p < 0.05 versus $CD34^{lo}$; #p < 0.05 versus $CD34^{hi}$.

(B and C) Adipogenic gene expression of the *in vitro* differentiated APCs (adipocytes) obtained from VAT, ASAT, and GFAT (n = 3 patient-matched APC subtypes per depot; passage 1 cells).

(B) *PPARγ*.

(C) *PLIN1*. *p < 0.05 versus day 0 within the same APC subtype; #p < 0.05 versus $CD34^{hi}$ at the same time point (passage 2 cells).

(D) Immunofluorescence staining showing lipid droplets (red) surrounded by PLIN1 protein (green) in adipocytes derived from different APC subtypes. Cells were obtained from VAT, ASAT, and GFAT at passage 2. Representative image of n = 3 independent experiments. Scale bar: 50 μm

(E) Triglyceride content in APC-derived adipocytes (n = 6 patient-matched APC subtypes from n = 3 from ASAT and n = 3 from GFAT). Above: representative images of cells stained with Oil Red O corresponding to the ASAT APC subtype identified in the figure.

(F) Adiponectin secretion into the culture medium (n = 5 subject-matched APC subtypes).

Data are presented as means ± SEM. Statistical significance was evaluated by two-way ANOVA with Bonferroni test for multiple comparisons using patient-matched data (A–C) or one-way Friedman test with Dunn's multiple comparison using patient-matched data (E). See also Figure S3.

identified fibro-adipogenic CD9 high progenitor cells were characterized by higher expression of fibrosis genes (Marcelin et al., 2017). Although gene expression of pro-fibrotic genes was lower in $CD34^{lo}$ APCs, none of the APC subsets identified in this analysis exhibited marked and consistent upregulation of fibrosis genes (Figure S2J). Taken together, these data suggest that the APCs identified in this analysis are distinct from those identified by Marcelin et al. (2017).

Unbiased Gene Expression Analysis Confirms Distinct Pools of Adipocyte Progenitors

To investigate the molecular identity of the APCs, RNA was extracted from freshly sorted APC subtypes obtained from the VAT of patients and subjected to RNA-seq analysis. An average of 16.8 million sequence reads were mapped to the human genome and 14,027 genes were identified (Table S2). Analysis of differentially expressed genes shows that the APC subtypes are related but distinct. We identified 1,389 and 2,013 genes showing significant expression changes between $CD34^{hi}$ cells and $CD34^{lo}$ and $CD34^{-}$ cells, respectively, and 401 differentially expressed genes when comparing $CD34^{lo}$ and $CD34^{-}$ cells (Table S2; Figure S2K). Practically all of the differentially regulated genes had a logFC > 3, demonstrating highly significant differences in gene expression between APC populations (Figure S2K). Unsupervised hierarchical clustering of the differentially expressed genes showed distinct clustering of the $CD34^{hi}$ cells (Figure 1H). The $CD34^{lo}$ and $CD34^{-}$ APCs were also clustered into their respective groups. Principal-component analysis highlights the separation of $CD34^{hi}$ APCs from the other APCs in the first dimension and separation of $CD34^{lo}$ and $CD34^{-}$ APCs in the second dimension (Figure 1I). These molecular data support the notion that there is significant heterogeneity of APCs within the same adipose tissue depot.

APCs Are Capable of Adipogenesis and Lipid Loading

The isolated cells maintained a fibroblast-like morphology in culture (Figure S2B) and the proliferative capacities of the APCs were similar, with the exception of $CD34^{-}$ cells derived from VAT, which were more proliferative than both $CD34^{hi}$ and $CD34^{lo}$ cells (Figure 2A). The three APC subtypes demonstrated a high adipogenic capacity upon exposure to a standard adipogenic differentiation protocol. There was a strong induction of

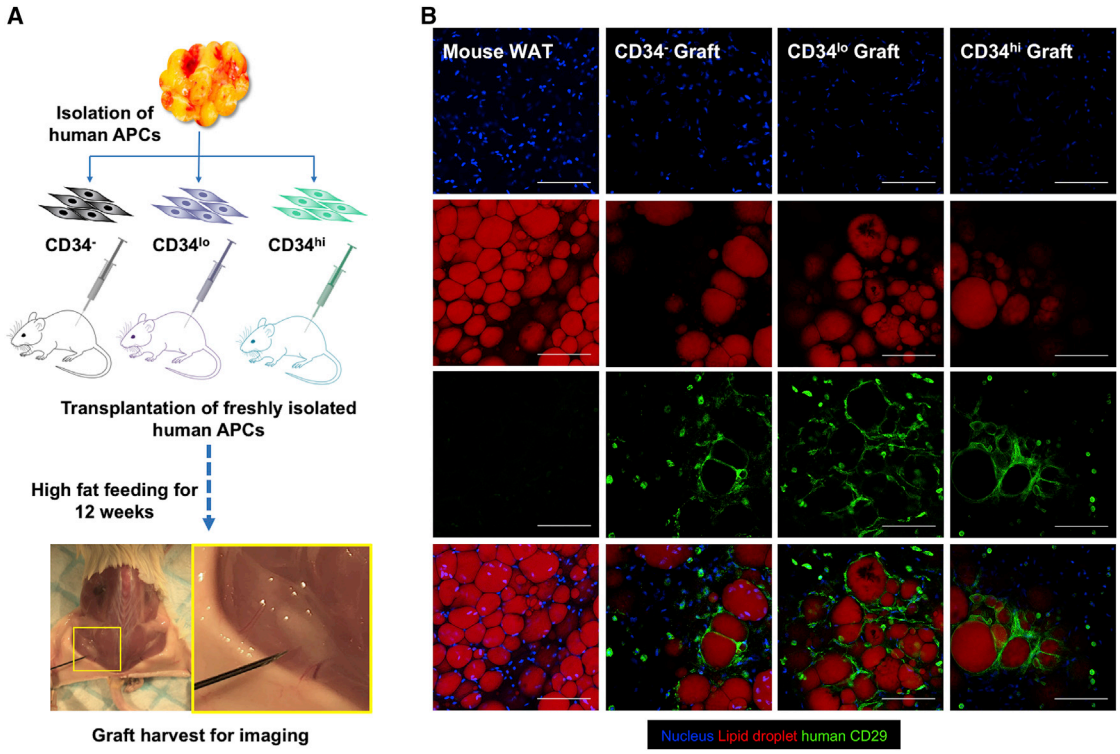

Figure 3. Human APCs Undergo Adipogenesis *In Vivo*

(A) Overview of xenotransplant experiment to assess APC adipogenesis *in vivo*. Freshly sorted human APCs suspended in Matrigel were implanted subcutaneously into the dorsal flank of SCID mice. The mice were fed a high-fat diet for 12 weeks before harvest of the grafts. Location of the fat pad formed from the implanted CD34^{hi} APCs is highlighted by a needle within the yellow box.

(B) Representative whole-mount imaging of mouse adipose tissue and the APC-derived grafts showing the presence of implanted human APCs (green and blue) and mature adipocytes differentiated from the human APCs (red and green and blue). Green, antibody specific to human CD29; red, neutral lipids stained with BODIPY to identify mature adipocytes; blue, nuclear staining by DAPI. Scale bar: 100 μm.

See also Figure S4.

genes required for adipocyte commitment, such as *PPARγ* and *CEBPα* (Figures 2B and S3A), and upregulation of genes enriched in terminally differentiated white adipocytes including *PLIN1* and *FABP4* (Figures 2C and S3B). A hallmark of adipocytes is the localization of PLIN1 around intracellular lipid droplets. Immunohistochemical analysis showed the presence of PLIN1 surrounding lipid droplets in all differentiated APC subtypes obtained from each anatomical location (Figures 2D and S3C). The proportion of APCs that differentiated into adipocytes was determined by counting the number of cells positively stained with Oil Red O, and this averaged ~80% across all APC subtypes, with no significant differences between subtypes obtained from different anatomical locations (Figure S3D). Adipocyte differentiation was also confirmed using PLIN1 immunostaining and yielded similar results (see Figure S3C for representative image). In agreement with the immunohistochemistry data, triglyceride levels in adipocytes derived from different APC subtypes of subcutaneous adipose tissues were not different (Figure 2E). Finally, all differentiated APCs secreted adiponectin, further confirming adipogenesis *in vitro* (Figure 2F). We were unable to culture the remaining Lin$^-$ stromal cells (i.e., cells present but not identified as APCs in Figure 1C) using the same growth medium, suggesting that the majority of the APCs are most likely confined to the identified populations.

APCs Undergo Adipogenesis *In Vivo*

APCs undergo adipogenesis when exposed to an appropriate set of cues, which are dictated by the tissue niche *in vivo*. Accordingly, we transplanted freshly isolated APC subtypes in close proximity to subcutaneous adipose in the dorsal flank of immunodeficient mice (Figure 3A). APCs from each subtype formed a fat pad (Figure 3A), and whole-mount confocal imaging of the grafts demonstrated the presence of lipid-filled cells with clear adipocyte morphology that were also positive for human CD29 (Figure 3B). We confirmed that these were adipocytes by PLIN1 immunostaining, which were also positively stained with human CD29 (Figure S4A). Successful grafting was confirmed for all APC subtypes obtained from four independent donors. Non-human adipocytes were also present in the xenografts (Figures 3B and S4B), which is due to the infiltration and differentiation of murine APCs into Matrigel, as reported previously (Lee et al., 2012; Tang et al., 2008). Together, these data demonstrate differentiation of each APC subtype into mature adipocytes *in vivo*.

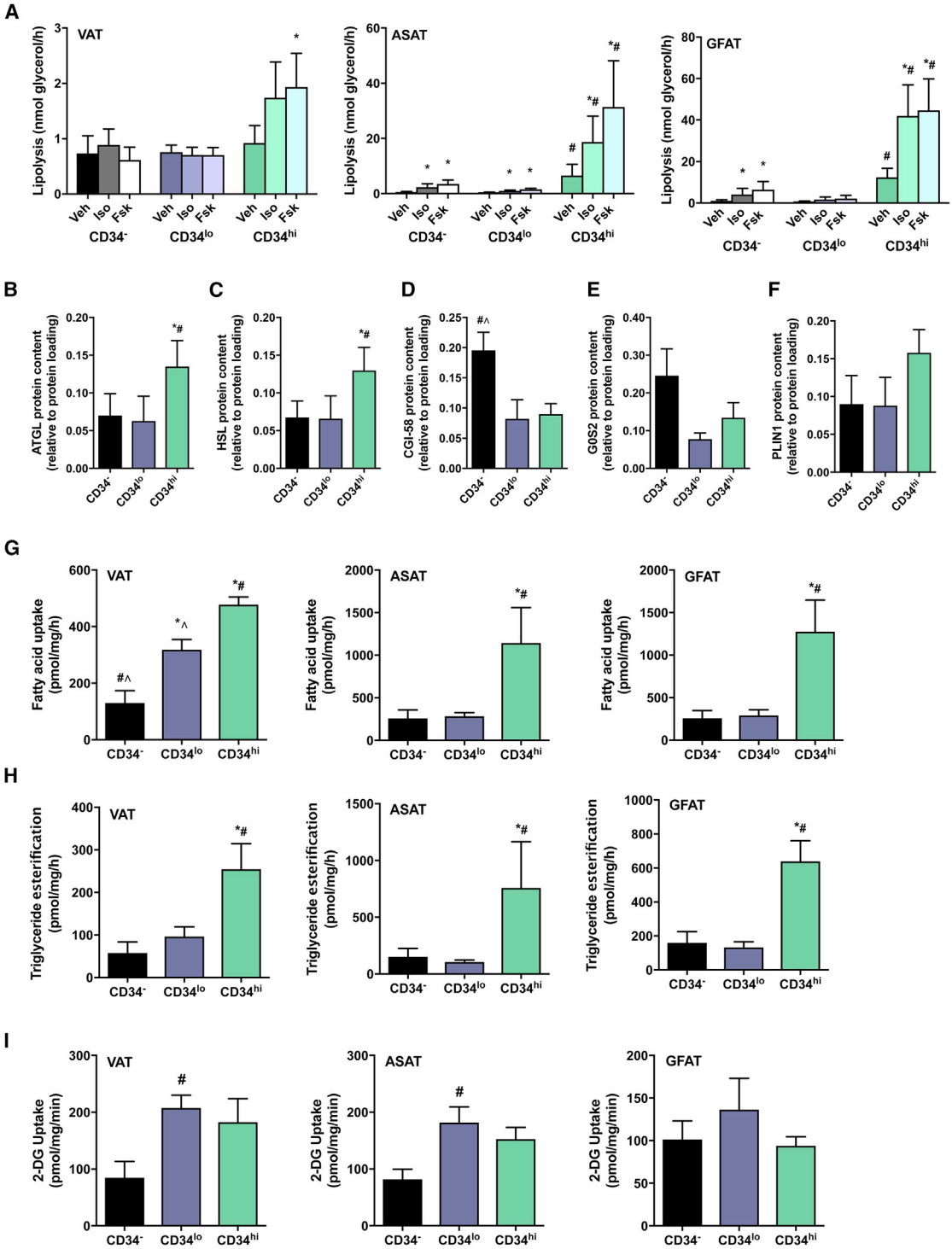

Figure 4. Metabolic Characterization of Adipocytes Derived from Human APC Subtypes

(A) Lipolysis as determined by glycerol release from adipocytes from differentiated APC subtypes derived from VAT, ASAT, and GFAT under basal and stimulated (ISO: 1 μM isoproterenol; Fsk: 20 μM forskolin) conditions. n = 5 subjects per adipocyte subtype per depot (passage 2). Data are means ± SEM. Statistical significance was evaluated by two-way ANOVA with Bonferroni test for multiple comparisons using patient-matched data. *$p < 0.05$ versus Veh within the same group; $^{\#}p < 0.05$ $CD34^{hi}$ versus $CD34^{-}$ and $CD34^{lo}$ within the same treatment condition.

(B–F) Contents of proteins involved in lipolysis. ATGL (B), HSL (C), CGI-58 (D), G0S2 (E), and PLIN1 (F) in adipocytes from APC subtypes derived from ASAT (passage 2). The immunoblots were normalized to total protein loading for each sample, which was obtained by visualization and quantification of the stain-free blot image. n = 5 subject matched adipocyte subtypes per depot.

(legend continued on next page)

Human APCs Give Rise to Adipocytes with Distinct Metabolic Capacities

Adipocytes located in different regions of the body differ from one another with respect to metabolic function (Arner, 2005; Jensen, 2008; Tchernof et al., 2006), and there is evidence of slowly and rapidly replenishing metabolic pools in the adipose tissue (Ekstedt and Olivecrona, 1970). This suggests that adipocyte subtypes of varied metabolic capacities might co-exist in the same individual adipose tissue depot. Supporting this notion, Ingenuity Pathway Analysis of the APC subtype transcriptomes revealed differential expression of genes involved in metabolism and processes that impact metabolism (Table S3). Subsequent functional analysis demonstrated that the adipocytes derived from APCs exhibit metabolic heterogeneity and are characterized by differing lipid turnover rates.

All functional analyses were conducted in differentiated APCs, which are referred to herein as adipocytes. There was no significant difference in basal lipolysis in $CD34^{-}$, $CD34^{lo}$, and $CD34^{hi}$ adipocytes derived from VAT, and the pan-β-adrenergic agonist isoproterenol did not increase lipolysis in any VAT adipocyte type (Figure 4A). This was unlikely to result from defective signaling through the adrenoreceptors because forskolin, a chemical activator of protein kinase A (PKA) that induces its response distal to the β-adrenoreceptors, also failed to increase lipolysis in adipocytes derived from VAT. The most striking finding was that the rate of basal and stimulated lipolysis was ~15 times higher in ASAT and GFAT-derived $CD34^{hi}$ adipocytes compared with $CD34^{-}$ and $CD34^{lo}$ adipocytes from the same depot (Figure 4A). Lipolysis tended to be higher in $CD34^{-}$ compared with $CD34^{lo}$ adipocytes derived from ASAT and GFAT. Consistent with the marked increase in lipolysis in $CD34^{hi}$ adipocytes, protein abundance of ATGL and HSL, the lipases that catalyze the cleavage of fatty acids from the triglyceride molecule (Raajendiran et al., 2016), were increased in $CD34^{hi}$ compared with $CD34^{-}$ and $CD34^{lo}$ adipocytes (Figures 4B and 4C). CGI-58 binds to and activates ATGL in adipocytes (Lass et al., 2006), and CGI-58 protein was increased in $CD34^{-}$ adipocytes compared with $CD34^{hi}$ and $CD34^{-}$ adipocytes (Figure 4D). G0S2 is a negative regulator of ATGL activity (Yang et al., 2010), and its protein expression tended ($p = 0.12$) to be lower in $CD34^{hi}$ and $CD34^{lo}$ adipocytes compared with $CD34^{-}$ adipocytes (Figure 4E), while PLIN1 protein content was not different between groups (Figure 4F). Representative immunoblots are shown in Figure S5A. The higher CGI-58 expression in $CD34^{-}$ adipocytes was surprising in light of the low lipolytic rates in these adipocytes. We speculate that the high expression of CGI-58 in $CD34^{-}$ adipocytes does not result in high lipolytic rates because ATGL and HSL protein contents are low and G0S2 content is high (Figures 4B–4E). Alternatively, CGI-58 has ATGL-independent functions, such as lysophosphatidic acid acyltransferase activity and lipid-signaling functions, and these might be more important in certain adipocyte subtypes (i.e., distinct roles for alpha-beta hydrolase domain 5 [ABHD5/CGI-58] and adipose triglyceride lipase [ATGL/PNPLA2] in lipid metabolism and signaling) (Lord and Brown, 2012).

[1-^{14}C]Oleate was used to determine the rate of fatty acid uptake and triglyceride esterification in adipocytes. Fatty acid uptake was increased in the $CD34^{lo}$ and $CD34^{hi}$ adipocytes compared with the $CD34^{-}$ adipocytes obtained from VAT (Figure 4G). In ASAT and GFAT, fatty acid uptake was increased by ~400% in $CD34^{hi}$ adipocytes when compared with the corresponding $CD34^{-}$ and $CD34^{lo}$ adipocytes (Figure 4G). The rates of the incoming fatty acids into triglyceride esterification mirrored the rates of fatty acid uptake (Figure 4H). Together, these data demonstrate that $CD34^{hi}$ adipocytes possess markedly higher lipid turnover compared with $CD34^{-}$ and $CD34^{lo}$ adipocytes and further suggest that the metabolic features of adipocytes are not strongly regulated by the anatomical location of the tissue they originate from.

In contrast to the marked variation in lipid flux between different adipocytes, the cell-intrinsic differences in glucose uptake were less pronounced. Glucose uptake by $CD34^{lo}$ adipocytes derived from ASAT and VAT was higher than $CD34^{-}$ adipocytes, and there was no difference in the rates of glucose uptake for the different adipocytes from GFAT (Figure 4I). Rates of *de novo* lipogenesis were very low in the APC-derived adipocytes and were generally not different between APC subtypes (Figure S5B).

Respiratory and Thermogenic Potential of the Different APC-Derived Adipocytes

"Beige" adipocytes reside within classical white adipose tissue depots and are characterized by their capacity to dissipate stored energy as heat through a process known as adaptive thermogenesis (Rosen and Spiegelman, 2014). High expression of CD29 on the cell surface of human pre-adipocytes predicts thermogenic capacity in mature adipocytes (Xue et al., 2015), and thermogenic activity is dependent on the master transcriptional regulator PR domain containing 16 (PRDM16) (Seale et al., 2007). In line with the differences in CD29 and *PRDM16* expression between the APC subtypes (i.e., $CD34^{-} > CD34^{hi} > CD34^{lo}$) (Table S2; Figures S6A and S6B), there was enrichment of beige adipocyte markers including *PPARGC1A* (encoding PGC1α), *CITED1*, *TCF21*, and *UCP1* in the $CD34^{-}$ adipocytes compared with $CD34^{lo}$ and $CD34^{hi}$ adipocytes derived from ASAT (Figures 5A–5D). These transcripts were markedly upregulated in response to β-adrenergic stimulation in $CD34^{-}$ adipocytes only, indicating induction of these adipocytes to a beige-like phenotype. Direct measurement of mitochondrial respiration showed that adipocytes derived from $CD34^{-}$ APCs obtained from ASAT recapitulate beige-adipocyte functions characterized by an increase in basal respiration and proton leak in response to

(G and H) Fatty acid metabolism in adipocytes from APC subtypes derived from VAT, ASAT, and GFAT (passage 2).
(G) Fatty acid uptake.
(H) Fatty acid esterification. n = 5 subjects per adipocyte subtype per depot.
(I) 2-Deoxyglucose uptake in adipocytes from APC subtypes derived from VAT, ASAT, and GFAT (passage 2). n = 5 subjects per adipocyte subtype per depot.
For (B)–(I), data are means ± SEM. Statistical significance was evaluated by one-way Friedman test with Dunn's multiple comparison. *$p < 0.05$ versus $CD34^{-}$, $^{\#}p < 0.05$ versus $CD34^{lo}$, and $^{\wedge}p < 0.05$ versus $CD34^{hi}$. See also Figure S5.

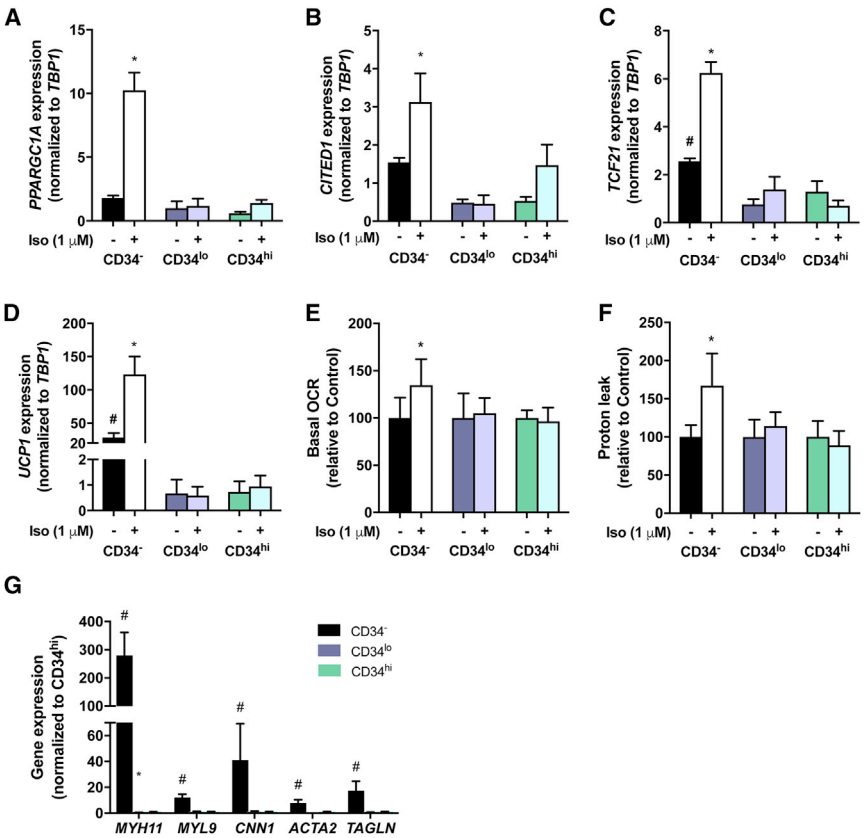

Figure 5. Evidence That CD34⁻ APCs Give Rise to Beige Adipocytes

(A–D) mRNA expression of beige adipocyte markers in cells treated without (–) or with 1 μM isoproterenol (+) in adipocytes from APC subtypes derived from ASAT (passage 2, n = 3 subject matched adipocyte subtypes). *PPARGC1A* (A), *CITED1* (B), *TCF21* (C), and *UCP1* (D). Statistical significance was evaluated by two-way ANOVA with Bonferroni test for multiple comparisons using patient-match data. *p < 0.05 versus –Iso within the same group; #p < 0.05 versus –Iso between groups.

(E and F) Oxygen consumption rates in adipocytes from differentiated APC subtypes derived from ASAT and GFAT.

(E) Basal and isoproterenol-stimulated oxygen consumption rate (OCR).

(F) Proton leak in the absence and presence of isoproterenol (n = 4 independent subjects). Statistical significance was evaluated by two-way ANOVA with Bonferroni test for multiple comparisons. *p < 0.05 versus –Iso within the same group.

(G) mRNA expression of smooth muscle cell-like markers in freshly isolated APCs (RNA-seq analysis). Statistical significance for individual genes was evaluated by one-way ANOVA with Bonferroni test for multiple comparisons. #p < 0.05 versus $CD34^{lo}$ and $CD34^{hi}$. *p < 0.05 versus $CD34^{hi}$.

See also Figure S6.

β-adrenergic stimulation (Figures 5E and 5F). Similarly, $CD34^{-}$ adipocytes derived from VAT APCs had increased expression of *PPARGC1A* and *UCP1* when compared with $CD34^{hi}$ adipocytes, while *CITED1* and *TCF21* expression were not different (Figures S6C–S6F). *PPARGC1A* and *UCP1* expression was markedly upregulated in response to β-adrenergic stimulation in $CD34^{-}$ adipocytes (Figures S6C and S6D) and was accompanied by an increase in proton leak without increments in basal respiration (Figures S6G and S6H). Such effects were not apparent in the $CD34^{lo}$ and $CD34^{hi}$ adipocytes. Previous studies have shown that a subset of beige adipocytes express smooth muscle linage-selective genes (Long et al., 2014) and that a similar subset of genes was abundantly expressed in clonal human brown preadipocyte cells (Shinoda et al., 2015). In further supporting the likelihood that $CD34^{-}$ APCs are beige adipocyte progenitors, $CD34^{-}$ APCs were highly enriched with this same subset of smooth muscle-like genes including *MYH11*, *MYL9*, *CNN1*, *ACTA2*, and *TAGLN* (Figure 5G). Together, these data demonstrate that $CD34^{-}$ APCs are likely progenitors for beige-like adipocytes in various human white adipose tissue depots, supporting the potential for "beigeing" in both subcutaneous and visceral depots.

Protein Secretion from Adipocyte Subtypes

Adipocytes are highly secretory cells (Crowe et al., 2009), and we extended our analysis examining adipocyte heterogeneity to protein secretion. We identified 742 secreted proteins across all the samples using a data-dependent acquisition liquid chromatography-tandem mass spectrometry (LC-MS/MS) approach and 79% of these were identified by gene ontology (GO) as localized to the extracellular region (GO:0005576), indicating that these are likely to be secreted proteins (Table S4). Of these, 269 proteins have a N-terminal signal peptide sequence, indicating that these are classically secreted proteins (Figure 6A; Table S4). The protein secretion profile was similar for $CD34^{hi}$ and $CD34^{lo}$ adipocytes, but there was a marked difference in the $CD34^{-}$ adipocyte secretome compared with the other adipocyte subtypes (Figures 6B and 6C). Only 32 proteins were differentially secreted between $CD34^{hi}$ and $CD34^{lo}$ adipocytes ($p < 0.05$, $Log_2FC > 1$), of which 84% were upregulated in $CD34^{lo}$ adipocytes (Figure 6D). There were 159 differentially secreted proteins when comparing the secretome of $CD34^{hi}$ and $CD34^{-}$ adipocytes (Figure 6E), and 176 differentially secreted proteins between $CD34^{lo}$ and $CD34^{-}$ adipocytes (Figure 6F). Ingenuity Pathway Analyses showed that the proteins secreted from $CD34^{hi}$ adipocytes (versus $CD34^{lo}$) are enriched in several canonical pathways including ceramide degradation, sphingosine and sphingosine-1-phosphate metabolism, and RhoGD1 signaling (Figure S7A). For $CD34^{-}$ APC-derived adipocytes (versus both $CD34^{hi}$ and $CD34^{lo}$), there is upregulation of interrelated canonical pathways for extracellular remodeling, LXR-RXR and FXR-RXR activation, and acute-phase signaling (Figures S7B and S7C). Together, these studies demonstrate that the APCs derived from CD34 expressing APCs have secretion

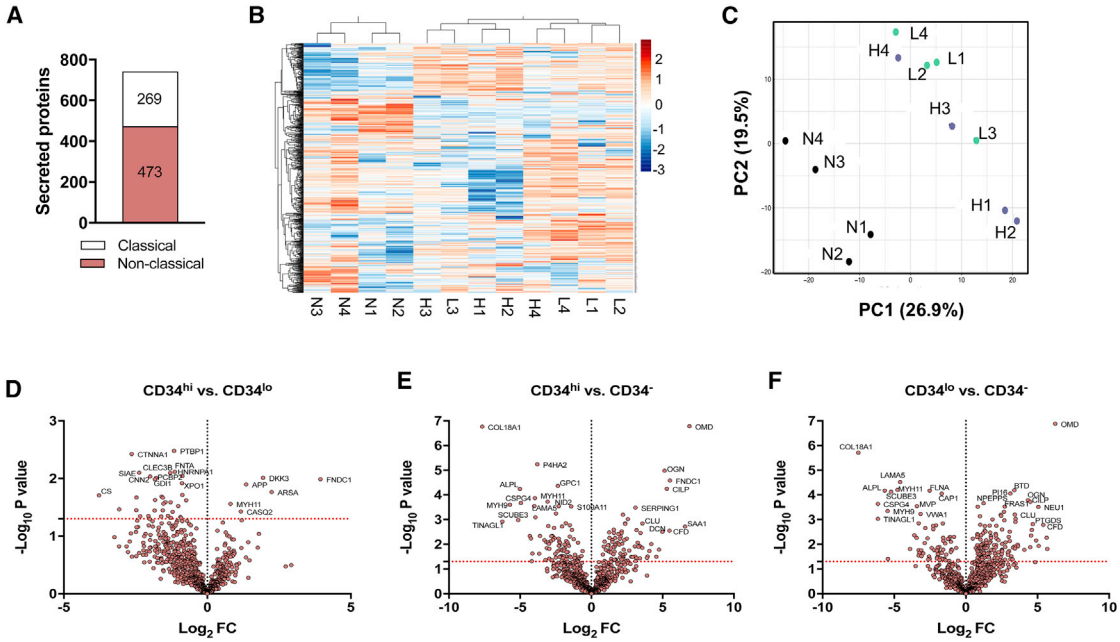

Figure 6. Protein Secretion Is Different between Adipocytes Derived from APC Subtypes

(A) Number of proteins secreted from adipocytes derived from APCs of ASAT. Classically secreted proteins are those harboring a N-terminal signal peptide.

(B) Heatmap and hierarchical clustering of proteomics data.

(C) Principal-component analysis highlighting clustering of APCs. H, CD34^{hi}; L, CD34^{lo}; N, CD34^{-}. Numbers after letters denote the patient number.

(D–F) Volcano plots showing differentially secreted proteins between (D) CD34^{hi} and CD34^{lo}, (E) CD34^{hi} and CD34^{-}, and (F) CD34^{lo} and CD34^{-}. Prominent upregulated and downregulated secreted proteins within each comparison are highlighted. Red line: adjusted $p < 0.05$; black line distinguishes the upregulated and downregulated proteins.

See also Figure S7 and Table S4.

profiles that are very different from adipocytes from CD34^{-} APCs and further highlight the heterogeneity in APC subtypes.

Remodeling of the APC Pool in Type 2 Diabetes Patients

Type 2 diabetes mellitus (T2DM) is associated with impaired lipid metabolism, which is highlighted by an increase in basal adipocyte lipolysis (Jocken et al., 2013). Given the different metabolic and endocrine profiles of the APC subtypes, we asked whether the distribution of APCs was altered in patients with T2DM. T2DM was of variable duration (6.9 ± 1.9 years) and patients were treated with lifestyle alone (n = 2), metformin (n = 3), combination therapy of metformin and a DPP4 inhibitor (n = 1), or metformin and insulin (n = 2). GFAT was not assessed due to insufficient tissue availability. Direct assessment of the APC distribution in T2DM patients and weight-matched individuals without T2DM (Table S5) showed that the proportion of CD34^{-} cells is significantly lower (4.2-fold) and the proportion of CD34^{hi} cells is significantly higher (4.1-fold) in T2DM (Figures 7A–7C).

DISCUSSION

The increased prevalence of obesity and associated metabolic diseases has fueled intense interest in understanding adipocyte development and function. While it is well known that a committed progenitor pool exists to generate new adipocytes and adipose tissue mass (Jeffery et al., 2016; Tchkonia et al., 2013), the identity of human APCs has remained elusive. In the present study, we have defined unique subtypes of human APCs that give rise to adipocytes with distinct metabolic and endocrine functions, and their distribution provides insights into the heterogeneity of human white adipose tissue.

Murine adipocytes are produced from a heterogeneous mix of APCs that reside in the same adipose tissue depot (Burl et al., 2018; Lee et al., 2017; Macotela et al., 2012; Sanchez-Gurmaches and Guertin, 2014; Schwalie et al., 2018). Several studies have shown that divergent human APC populations give rise to adipocytes with distinct molecular, proliferative, adipogenic, and thermogenic characteristics (Cawthorn et al., 2012; Ong et al., 2014; Tchkonia et al., 2005; Xue et al., 2015); however, a detailed molecular description of the putative APC subtypes and an understanding of their metabolic and endocrine phenotype is incomplete. Our FACS sorting and transcriptome analysis of freshly isolated stromal vascular fraction cells identified three molecularly distinct populations of human APCs that co-exist in similar ratios in the lineage depleted stromal vascular fraction of visceral and subcutaneous adipose tissues. These APCs exhibit similar capacities for proliferation, adipogenesis, and lipid loading *in vitro*, and, importantly, the freshly isolated APCs form mature adipocytes when transplanted into an adipogenic niche *in vivo*. The APC-derived adipocytes differ significantly in their metabolism and endocrine functions, with the most striking

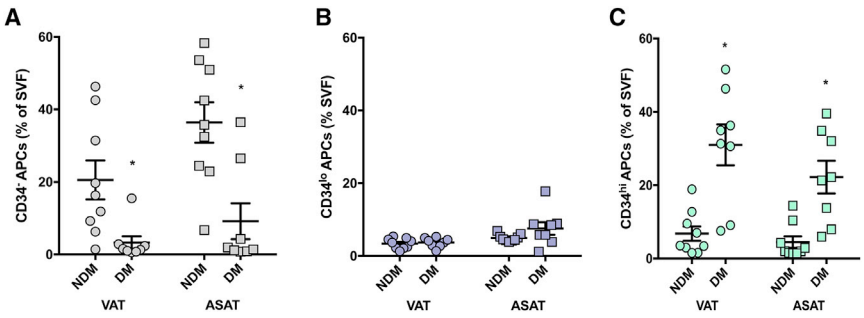

Figure 7. APC Distribution Is Altered in Patients with Type 2 Diabetes

Proportion of CD34$^-$ (A), CD34^{lo} (B), and CD34^{hi} (C) subtypes in human VAT and ASAT in patients with (DM) or without (NDM) type 2 diabetes. Individual data points reported with the mean ± SEM (n = 8 for DM; n = 9 for NDM). Statistical significance was evaluated by paired two-tailed t tests for comparison between NDM and DM for each adipose depot. *p < 0.05 versus NDM. See also Table S5.

observations being the remarkably high rates of lipolysis and fatty acid storage in the CD34^{hi}-derived adipocytes and the significant differences in protein secretion and beige-like phenotype of the CD34$^-$-derived adipocytes.

Adipose tissue is a critical regulator of whole-body metabolic homeostasis; however, not all adipose depots are functionally equivalent and the accumulation of excess visceral adipose tissue is strongly associated with higher incidence of cardiometabolic disease, whereas the accumulation of gluteofemoral adipose tissue is linked to protection against such diseases (Wajchenberg, 2000). These effects may be mediated by regional differences in adipocyte functions such as lipolysis, esterification, and adipokine secretion (Rosen and Spiegelman, 2014). Notable differences between mixed populations of human "pre-adipocytes" obtained from ASAT and VAT were previously reported, and include increased replicative and adipogenic capacities, reduced susceptibility to apoptosis, and altered gene expression with overrepresentation of developmental genes (Tchkonia et al., 2013). The present data show an increased number of APCs in gluteofemoral compared with visceral and subcutaneous abdominal adipose tissues, but similar distribution patterns of APC subtypes between these adipose tissue depots and similar metabolic traits of these APC subtypes, irrespective of their origin. Hence, intrinsic or "cell-autonomous" traits of adipocytes may not be the major determinant explaining the regional differences in adipose tissue metabolism in humans, but may explain the metabolic heterogeneity of adipocytes between individuals (Arner et al., 2018).

The present findings also bear relevance to the so-called adipose tissue expandability hypothesis, which posits that the capacity of adipose tissue to expand in response to positive energy balance facilitates safe storage of excess triglycerides, which in turn limits ectopic fat deposition (i.e., in muscle, liver) and associated metabolic and inflammatory derangements (Virtue and Vidal-Puig, 2010). Total APCs were increased by more than 60% in GFAT compared with VAT and ASAT. We postulate that the expanded reservoir of APCs in GFAT may explain the rapid creation of new adipocytes in lower-body compared with upper-body adipose tissue in response to overfeeding (Tchoukalova et al., 2010). Furthermore, the expanded reservoir of APCs may facilitate efficient adipogenesis and generation of small adipocytes, which is linked to the prevention of metabolic diseases (Sun et al., 2011), and may thereby provide a mechanistic explanation for the apparent cardiometabolic protection afforded by gluteofemoral adipose tissue.

The energy-dissipating properties of beige and/or brown adipocytes hold promise as a therapeutic modality against obesity and related complications (Harms and Seale, 2013), and identifying the human adipocyte populations capable of adaptive thermogenesis and their pathways of activation is of intense current interest. Fate-mapping studies have identified progenitor populations that give rise to brown and beige adipocytes in mice (Wang and Seale, 2016), and previous studies in mice (Lee et al., 2012) and humans (Xue et al., 2015) show that a subset of white adipose tissue-resident CD29$^+$ cells have thermogenic potential. Our data extend on these previous studies and show that the CD34$^-$ subset of CD29$^+$ APCs are progenitors of some beige adipocytes. CD34$^-$ APCs have the highest CD29 expression of the identified APCs; express the coregulatory protein PRDM16, which is required for development of beige adipocytes (Cohen et al., 2014); express genes of smooth muscle-like origin that are known to give rise to beige adipocytes (Burl et al., 2018; Shinoda et al., 2015); and, most importantly, produce adipocytes with beige-like features including the near absence of thermogenic genes under basal conditions and a strong induction during β-adrenergic stimulation, increased respiration in response to β-adrenergic stimulation, and gene expression distinct from that of the other APCs present in human white adipose tissue. The CD34$^-$ APCs are the most abundant subtype in the stromal vascular fraction of white adipose tissue and possess a molecular signature distinct from progenitors isolated from human supraclavicular brown adipose tissue (Shinoda et al., 2015), further supporting the likelihood that these are inducible progenitors. It has been reported that mouse inducible brown adipocyte progenitors are CD34$^+$ and express PDGFRα (Lee et al., 2012); however, *PDGFRA* was lowly expressed in the CD34$^-$ APCs compared with the other APC subtypes. Moreover, many beige/brown specific proteins previously identified in cultured preadipocyte lines derived from mice were not expressed in the human CD34$^-$ APCs (e.g., *Tbx1*, *Tmem26*, *CD137*, *P2rx5*; Table S2) (Ussar et al., 2014; Wu et al., 2012), indicating likely species differences in beige APCs. Taken together, our results identify an APC subtype that gives rise to a recruitable form of thermogenic adipocytes in humans. While the *in vivo* relevance of the CD34$^-$ APCs for human physiology is unresolved, the marked reduction of CD34$^-$ APCs in the adipose tissue of type 2 diabetes patients raises the intriguing possibility of impaired thermogenic potential in this population. Finally, a number of genes are uniquely expressed in CD34$^-$ APCs; however, it is not yet known whether these can serve as molecular markers

for the identification of thermogenic adipocytes *in vivo*, which will be the focus of future studies.

In considering the broader implications of this work, an understanding of an individual's APC composition may be useful for predicting metabolic and endocrine traits, and by extension, their suitability for therapeutic interventions. Basal lipolysis is increased in obesity and is closely associated with insulin resistance, and inhibition of adipocyte lipolysis is a promising therapeutic strategy for treating insulin resistance (Morigny et al., 2016; Schweiger et al., 2017). In this regard, deciphering the APC composition might be useful for identifying individuals at risk of high lipolysis and the development of metabolic disease, as shown here in type 2 diabetes patients that were characterized by significant increases in $CD34^{hi}$ and decreases in $CD34^{-}$ APCs. Future prospective cohort studies will evaluate the prognostic value of such information.

In summary, the results described here provide an advance in the understanding of human adipocyte function by demonstrating the existence of molecularly distinct APCs that give rise to adipocytes with unique metabolic and endocrine capacities. The variable distribution of these APCs between adipose tissue depots, and indeed between individuals, provides a conceptual framework for understanding the heterogeneity of human white adipose tissue. Harnessing the capabilities of specific APCs may have implications for the effective treatment of obesity and its related metabolic complications.

STAR★METHODS

Detailed methods are provided in the online version of this paper and include the following:

- KEY RESOURCES TABLE
- CONTACT FOR REAGENT AND RESOURCE SHARING
- EXPERIMENTAL MODEL AND SUBJECT DETAILS
  - Human studies
  - Animal studies
- METHOD DETAILS
  - White adipose tissue collection
  - Isolation of the stromal vascular fraction and sorting of APCs
  - Antibody staining and FACS
  - Histological analysis of human adipose tissue
  - Transcriptomic profiling of APCs
  - Culturing of sorted APCs
  - Assessment of cell proliferation
  - Adipogenic differentiation
  - Xenotransplantation of APCs
  - Whole-mount imaging of the graft
  - Immunohistochemistry of the graft
  - Gene expression analysis
  - Immunofluorescence microscopy
  - Immunoblot analysis
  - Metabolic assessments
  - Measurement of fatty acid metabolism
  - Measurement of glucose uptake
  - Measurement of mitochondrial respiration
  - Secretome analysis
- QUANTIFICATION AND STATISTICAL ANALYSIS
- DATA AND SOFTWARE AVAILABILITY

SUPPLEMENTAL INFORMATION

Supplemental Information can be found online at https://doi.org/10.1016/j.celrep.2019.04.010.

ACKNOWLEDGMENTS

We thank Jennifer Lo, Natalie Payne, Guizhi Sun, Claude Bernard (Monash University), and Sean McGee (Deakin University) for technical advice and reagents; Roxane Legae and Trevor Wilson (Hudson Institute) and Stuart K. Archer for assistance with the RNA-seq analysis; Kalai Shaw and the surgical and nursing staff at the Alfred Hospital; Andrew Fryga, Michael Reitsma, Adam Dinsdale, and Katherine Flanagan (Monash Flow Core), and Vanta Jameson and Joshua Kie (Melbourne Brain Centre Flow Cytometry Facility) for assistance with flow cytometry; Monash Micro Imaging and the Biological Optical Microscopy Platform (University of Melbourne) for assistance with confocal microscopy; and Graham Hepworth (University of Melbourne) for statistical consultancy. This work was supported by the National Health and Medical Research Council of Australia (NHMRC) (APP1098972) and the Monash Yale Strategic Grant in Metabolism (MDO17P01W). A.R. was supported by a scholarship from the Department of Physiology, Monash University. M.J.W. is supported by a Senior Research Fellowship from the NHMRC (APP1077703). R.A.T. is supported by the Victorian Cancer Agency (MCRF15023).

AUTHOR CONTRIBUTIONS

Conceptualization, A.R., M.S.R., and M.J.W.; Methodology, A.R. and R.A.T.; Investigation, A.R., J.B., A.K.C., R.B.S., R.A.T., and M.J.W.; Resources, G.O., P.E.O., and P.R.B.; Writing – Original Draft, A.R. and M.J.W.; Writing – Review & Editing, A.R., G.O., P.E.O., R.A.T., M.S.R., P.R.B., and M.J.W.; Visualization, A.R., R.A.T., and M.J.W.; Supervision, R.A.T., M.S.R., and M.J.W.; Funding Acquisition, P.E.O., M.S.R., and M.J.W.

DECLARATION OF INTERESTS

The authors declare no competing interests.

Received: April 8, 2018
Revised: March 18, 2019
Accepted: April 1, 2019
Published: April 30, 2019

REFERENCES

Acosta, J.R., Joost, S., Karlsson, K., Ehrlund, A., Li, X., Aouadi, M., Kasper, M., Arner, P., Rydén, M., and Laurencikiene, J. (2017). Single cell transcriptomics suggest that human adipocyte progenitor cells constitute a homogeneous cell population. Stem Cell Res. Ther. *8*, 250.

Adiconis, X., Borges-Rivera, D., Satija, R., DeLuca, D.S., Busby, M.A., Berlin, A.M., Sivachenko, A., Thompson, D.A., Wysoker, A., Fennell, T., et al. (2013). Comparative analysis of RNA sequencing methods for degraded or low-input samples. Nat. Methods *10*, 623–629.

Afshin, A., Forouzanfar, M.H., Reitsma, M.B., Sur, P., Estep, K., Lee, A., Marczak, L., Mokdad, A.H., Moradi-Lakeh, M., Naghavi, M., et al.; GBD 2015 Obesity Collaborators (2017). Health effects of overweight and obesity in 195 countries over 25 years. N. Engl. J. Med. *377*, 13–27.

Arner, P. (2005). Human fat cell lipolysis: biochemistry, regulation and clinical role. Best Pract. Res. Clin. Endocrinol. Metab. *19*, 471–482.

Arner, P., Andersson, D.P., Backdahl, J., Dahlman, I., and Ryden, M. (2018). Weight gain and impaired glucose metabolism in women are predicted by inefficient subcutaneous fat cell lipolysis. Cell Metab. *28*, 45–54.e3.

Berry, R., and Rodeheffer, M.S. (2013). Characterization of the adipocyte cellular lineage in vivo. Nat. Cell Biol. *15*, 302–308.

Berry, R., Church, C.D., Gericke, M.T., Jeffery, E., Colman, L., and Rodeheffer, M.S. (2014a). Imaging of adipose tissue. Methods Enzymol. *537*, 47–73.

Berry, R., Jeffery, E., and Rodeheffer, M.S. (2014b). Weighing in on adipocyte precursors. Cell Metab. *19*, 8–20.

Blüher, M., Patti, M.E., Gesta, S., Kahn, B.B., and Kahn, C.R. (2004). Intrinsic heterogeneity in adipose tissue of fat-specific insulin receptor knock-out mice is associated with differences in patterns of gene expression. J. Biol. Chem. *279*, 31891–31901.

Bullard, J.H., Purdom, E., Hansen, K.D., and Dudoit, S. (2010). Evaluation of statistical methods for normalization and differential expression in mRNA-seq experiments. BMC Bioinformatics *11*, 94.

Burl, R.B., Ramseyer, V.D., Rondini, E.A., Pique-Regi, R., Lee, Y.H., and Granneman, J.G. (2018). Deconstructing adipogenesis induced by beta3-adrenergic receptor activation with single-cell expression profiling. Cell Metab. *28*, 300–309.e4.

Cawthorn, W.P., Scheller, E.L., and MacDougald, O.A. (2012). Adipose tissue stem cells meet preadipocyte commitment: going back to the future. J. Lipid Res. *53*, 227–246.

Chau, Y.Y., Bandiera, R., Serrels, A., Martínez-Estrada, O.M., Qing, W., Lee, M., Slight, J., Thornburn, A., Berry, R., McHaffie, S., et al. (2014). Visceral and subcutaneous fat have different origins and evidence supports a mesothelial source. Nat. Cell Biol. *16*, 367–375.

Church, C.D., Berry, R., and Rodeheffer, M.S. (2014). Isolation and study of adipocyte precursors. Methods Enzymol. *537*, 31–46.

Clark, A.M., Sousa, K.M., Jennings, C., MacDougald, O.A., and Kennedy, R.T. (2009). Continuous-flow enzyme assay on a microfluidic chip for monitoring glycerol secretion from cultured adipocytes. Anal. Chem. *81*, 2350–2356.

Cohen, P., Levy, J.D., Zhang, Y., Frontini, A., Kolodin, D.P., Svensson, K.J., Lo, J.C., Zeng, X., Ye, L., Khandekar, M.J., et al. (2014). Ablation of PRDM16 and beige adipose causes metabolic dysfunction and a subcutaneous to visceral fat switch. Cell *156*, 304–316.

Conesa, A., Madrigal, P., Tarazona, S., Gomez-Cabrero, D., Cervera, A., McPherson, A., Szcześniak, M.W., Gaffney, D.J., Elo, L.L., Zhang, X., and Mortazavi, A. (2016). A survey of best practices for RNA-seq data analysis. Genome Biol. *17*, 13.

Crowe, S., Wu, L.E., Economou, C., Turpin, S.M., Matzaris, M., Hoehn, K.L., Hevener, A.L., James, D.E., Duh, E.J., and Watt, M.J. (2009). Pigment epithelium-derived factor contributes to insulin resistance in obesity. Cell Metab. *10*, 40–47.

Dobin, A., Davis, C.A., Schlesinger, F., Drenkow, J., Zaleski, C., Jha, S., Batut, P., Chaisson, M., and Gingeras, T.R. (2013). STAR: ultrafast universal RNA-seq aligner. Bioinformatics *29*, 15–21.

Ekstedt, B., and Olivecrona, T. (1970). Uptake and release of fatty acids by rat adipose tissue: last in to first out? Lipids *5*, 858–860.

Escher, C., Reiter, L., MacLean, B., Ossola, R., Herzog, F., Chilton, J., MacCoss, M.J., and Rinner, O. (2012). Using iRT, a normalized retention time for more targeted measurement of peptides. Proteomics *12*, 1111–1121.

Fang, L., Guo, F., Zhou, L., Stahl, R., and Grams, J. (2015). The cell size and distribution of adipocytes from subcutaneous and visceral fat is associated with type 2 diabetes mellitus in humans. Adipocyte *4*, 273–279.

Gao, H., Volat, F., Sandhow, L., Galitzky, J., Nguyen, T., Esteve, D., Åström, G., Mejhert, N., Ledoux, S., Thalamas, C., et al. (2017). CD36 is a marker of human adipocyte progenitors with pronounced adipogenic and triglyceride accumulation potential. Stem Cells *35*, 1799–1814.

Harms, M., and Seale, P. (2013). Brown and beige fat: development, function and therapeutic potential. Nat. Med. *19*, 1252–1263.

Jeffery, E., Wing, A., Holtrup, B., Sebo, Z., Kaplan, J.L., Saavedra-Peña, R., Church, C.D., Colman, L., Berry, R., and Rodeheffer, M.S. (2016). The adipose tissue microenvironment regulates depot-specific adipogenesis in obesity. Cell Metab. *24*, 142–150.

Jensen, M.D. (2008). Role of body fat distribution and the metabolic complications of obesity. J. Clin. Endocrinol. Metab. *93* (*11, Suppl 1*), S57–S63.

Jocken, J.W., Goossens, G.H., Boon, H., Mason, R.R., Essers, Y., Havekes, B., Watt, M.J., van Loon, L.J., and Blaak, E.E. (2013). Insulin-mediated suppression of lipolysis in adipose tissue and skeletal muscle of obese type 2 diabetic men and men with normal glucose tolerance. Diabetologia *56*, 2255–2265.

Lass, A., Zimmermann, R., Haemmerle, G., Riederer, M., Schoiswohl, G., Schweiger, M., Kienesberger, P., Strauss, J.G., Gorkiewicz, G., and Zechner, R. (2006). Adipose triglyceride lipase-mediated lipolysis of cellular fat stores is activated by CGI-58 and defective in Chanarin-Dorfman Syndrome. Cell Metab. *3*, 309–319.

Law, C.W., Chen, Y., Shi, W., and Smyth, G.K. (2014). voom: precision weights unlock linear model analysis tools for RNA-seq read counts. Genome Biol. *15*, R29.

Lee, M.J., and Fried, S.K. (2014). Optimal protocol for the differentiation and metabolic analysis of human adipose stromal cells. Methods Enzymol. *538*, 49–65.

Lee, Y.H., Petkova, A.P., Mottillo, E.P., and Granneman, J.G. (2012). In vivo identification of bipotential adipocyte progenitors recruited by β3-adrenoceptor activation and high-fat feeding. Cell Metab. *15*, 480–491.

Lee, Y.H., Kim, S.N., Kwon, H.J., and Granneman, J.G. (2017). Metabolic heterogeneity of activated beige/brite adipocytes in inguinal adipose tissue. Sci. Rep. *7*, 39794.

Liao, Y., Smyth, G.K., and Shi, W. (2014). featureCounts: an efficient general purpose program for assigning sequence reads to genomic features. Bioinformatics *30*, 923–930.

Long, J.Z., Svensson, K.J., Tsai, L., Zeng, X., Roh, H.C., Kong, X., Rao, R.R., Lou, J., Lokurkar, I., Baur, W., et al. (2014). A smooth muscle-like origin for beige adipocytes. Cell Metab. *19*, 810–820.

Lord, C.C., and Brown, J.M. (2012). Distinct roles for alpha-beta hydrolase domain 5 (ABHD5/CGI-58) and adipose triglyceride lipase (ATGL/PNPLA2) in lipid metabolism and signaling. Adipocyte *1*, 123–131.

Macotela, Y., Emanuelli, B., Mori, M.A., Gesta, S., Schulz, T.J., Tseng, Y.H., and Kahn, C.R. (2012). Intrinsic differences in adipocyte precursor cells from different white fat depots. Diabetes *61*, 1691–1699.

Marcelin, G., Ferreira, A., Liu, Y., Atlan, M., Aron-Wisnewsky, J., Pelloux, V., Botbol, Y., Ambrosini, M., Fradet, M., Rouault, C., et al. (2017). A PDGFRα-mediated switch toward $CD9^{high}$ adipocyte progenitors controls obesity-induced adipose tissue fibrosis. Cell Metab. *25*, 673–685.

Metsalu, T., and Vilo, J. (2015). ClustVis: a web tool for visualizing clustering of multivariate data using principal component analysis and heatmap. Nucleic Acids Res. *43* (*W1*), W566–W570.

Morigny, P., Houssier, M., Mouisel, E., and Langin, D. (2016). Adipocyte lipolysis and insulin resistance. Biochimie *125*, 259–266.

Ong, W.K., Tan, C.S., Chan, K.L., Goesantoso, G.G., Chan, X.H., Chan, E., Yin, J., Yeo, C.R., Khoo, C.M., So, J.B., et al. (2014). Identification of specific cell-surface markers of adipose-derived stem cells from subcutaneous and visceral fat depots. Stem Cell Reports *2*, 171–179.

Raajendiran, A., Tsiloulis, T., and Watt, M.J. (2016). Adipose tissue development and the molecular regulation of lipid metabolism. Essays Biochem. *60*, 437–450.

Rantalainen, M., Herrera, B.M., Nicholson, G., Bowden, R., Wills, Q.F., Min, J.L., Neville, M.J., Barrett, A., Allen, M., Rayner, N.W., et al. (2011). MicroRNA expression in abdominal and gluteal adipose tissue is associated with mRNA expression levels and partly genetically driven. PLoS ONE *6*, e27338.

Robinson, M.D., and Oshlack, A. (2010). A scaling normalization method for differential expression analysis of RNA-seq data. Genome Biol. *11*, R25.

Rodeheffer, M.S., Birsoy, K., and Friedman, J.M. (2008). Identification of white adipocyte progenitor cells in vivo. Cell *135*, 240–249.

Rosen, E.D., and Spiegelman, B.M. (2014). What we talk about when we talk about fat. Cell *156*, 20–44.

Sanchez-Gurmaches, J., and Guertin, D.A. (2014). Adipocytes arise from multiple lineages that are heterogeneously and dynamically distributed. Nat. Commun. *5*, 4099.

Schindelin, J., Arganda-Carreras, I., Frise, E., Kaynig, V., Longair, M., Pietzsch, T., Preibisch, S., Rueden, C., Saalfeld, S., Schmid, B., et al. (2012). Fiji: an open-source platform for biological-image analysis. Nat. Methods *9*, 676–682.

Schwalie, P.C., Dong, H., Zachara, M., Russeil, J., Alpern, D., Akchiche, N., Caprara, C., Sun, W., Schlaudraff, K.U., Soldati, G., et al. (2018). A stromal cell population that inhibits adipogenesis in mammalian fat depots. Nature *559*, 103–108.

Schweiger, M., Romauch, M., Schreiber, R., Grabner, G.F., Hütter, S., Kotzbeck, P., Benedikt, P., Eichmann, T.O., Yamada, S., Knittelfelder, O., et al. (2017). Pharmacological inhibition of adipose triglyceride lipase corrects high-fat diet-induced insulin resistance and hepatosteatosis in mice. Nat. Commun. *8*, 14859.

Seale, P., Kajimura, S., Yang, W., Chin, S., Rohas, L.M., Uldry, M., Tavernier, G., Langin, D., and Spiegelman, B.M. (2007). Transcriptional control of brown fat determination by PRDM16. Cell Metab. *6*, 38–54.

Shinoda, K., Luijten, I.H., Hasegawa, Y., Hong, H., Sonne, S.B., Kim, M., Xue, R., Chondronikola, M., Cypess, A.M., Tseng, Y.H., et al. (2015). Genetic and functional characterization of clonally derived adult human brown adipocytes. Nat. Med. *21*, 389–394.

Spalding, K.L., Arner, E., Westermark, P.O., Bernard, S., Buchholz, B.A., Bergmann, O., Blomqvist, L., Hoffstedt, J., Näslund, E., Britton, T., et al. (2008). Dynamics of fat cell turnover in humans. Nature *453*, 783–787.

Stein, Y., and Stein, O. (1961). Metabolic activity of rat epididymal fat pad labeled selectively by an in vivo incubation technique. Biochim. Biophys. Acta *54*, 555–571.

Sun, K., Kusminski, C.M., and Scherer, P.E. (2011). Adipose tissue remodeling and obesity. J. Clin. Invest. *121*, 2094–2101.

Tang, W., Zeve, D., Suh, J.M., Bosnakovski, D., Kyba, M., Hammer, R.E., Tallquist, M.D., and Graff, J.M. (2008). White fat progenitor cells reside in the adipose vasculature. Science *322*, 583–586.

Tariq, M.A., Kim, H.J., Jejelowo, O., and Pourmand, N. (2011). Whole-transcriptome RNAseq analysis from minute amount of total RNA. Nucleic Acids Res. *39*, e120.

Tchernof, A., Bélanger, C., Morisset, A.S., Richard, C., Mailloux, J., Laberge, P., and Dupont, P. (2006). Regional differences in adipose tissue metabolism in women: minor effect of obesity and body fat distribution. Diabetes *55*, 1353–1360.

Tchkonia, T., Tchoukalova, Y.D., Giorgadze, N., Pirtskhalava, T., Karagiannides, I., Forse, R.A., Koo, A., Stevenson, M., Chinnappan, D., Cartwright, A., et al. (2005). Abundance of two human preadipocyte subtypes with distinct capacities for replication, adipogenesis, and apoptosis varies among fat depots. Am. J. Physiol. Endocrinol. Metab. *288*, E267–E277.

Tchkonia, T., Thomou, T., Zhu, Y., Karagiannides, I., Pothoulakis, C., Jensen, M.D., and Kirkland, J.L. (2013). Mechanisms and metabolic implications of regional differences among fat depots. Cell Metab. *17*, 644–656.

Tchoukalova, Y.D., Votruba, S.B., Tchkonia, T., Giorgadze, N., Kirkland, J.L., and Jensen, M.D. (2010). Regional differences in cellular mechanisms of adipose tissue gain with overfeeding. Proc. Natl. Acad. Sci. USA *107*, 18226–18231.

Ussar, S., Lee, K.Y., Dankel, S.N., Boucher, J., Haering, M.F., Kleinridders, A., Thomou, T., Xue, R., Macotela, Y., Cypess, A.M., et al. (2014). ASC-1, PAT2, and P2RX5 are cell surface markers for white, beige, and brown adipocytes. Sci. Transl. Med. *6*, 247ra103.

Virtue, S., and Vidal-Puig, A. (2010). Adipose tissue expandability, lipotoxicity and the metabolic syndrome—an allostatic perspective. Biochim. Biophys. Acta *1801*, 338–349.

Wajchenberg, B.L. (2000). Subcutaneous and visceral adipose tissue: their relation to the metabolic syndrome. Endocr. Rev. *21*, 697–738.

Wang, W., and Seale, P. (2016). Control of brown and beige fat development. Nat. Rev. Mol. Cell Biol. *17*, 691–702.

Wu, J., Boström, P., Sparks, L.M., Ye, L., Choi, J.H., Giang, A.H., Khandekar, M., Virtanen, K.A., Nuutila, P., Schaart, G., et al. (2012). Beige adipocytes are a distinct type of thermogenic fat cell in mouse and human. Cell *150*, 366–376.

Xu, X., Wilschut, K.J., Kouklis, G., Tian, H., Hesse, R., Garland, C., Sbitany, H., Hansen, S., Seth, R., Knott, P.D., et al. (2015). Human satellite cell transplantation and regeneration from diverse skeletal muscles. Stem Cell Reports *5*, 419–434.

Xue, R., Lynes, M.D., Dreyfuss, J.M., Shamsi, F., Schulz, T.J., Zhang, H., Huang, T.L., Townsend, K.L., Li, Y., Takahashi, H., et al. (2015). Clonal analyses and gene profiling identify genetic biomarkers of the thermogenic potential of human brown and white preadipocytes. Nat. Med. *21*, 760–768.

Yang, X., Lu, X., Lombès, M., Rha, G.B., Chi, Y.I., Guerin, T.M., Smart, E.J., and Liu, J. (2010). The G_0/G_1 switch gene 2 regulates adipose lipolysis through association with adipose triglyceride lipase. Cell Metab. *11*, 194–205.

Zwiener, I., Frisch, B., and Binder, H. (2014). Transforming RNA-seq data to improve the performance of prognostic gene signatures. PLoS ONE *9*, e85150.

STAR★METHODS

KEY RESOURCES TABLE

REAGENT or RESOURCE	SOURCE	IDENTIFIER
Antibodies		
CD31	BD Biosciences	561653
CD45	BD Biosciences	641399
CD29	BD Biosciences	559883
CD34	BD Biosciences	348057
anti-PLIN1 antibody	Abcam	ab61682
donkey anti-goat antibody	ThermoFisher Scientific	A21084
anti-human CD29 antibody	Biolegend	303018
ATGL	Cell Signaling Technologies	2138 S
HSL	Cell Signaling Technologies	18381 S
CGI-58	Abcam	ab73551
GOS2	ProteinTech	12091-1-AP
Mouse anti-goat IgG-HRP	Santa Cruz	sc-2354
Amersham ECL Mouse IgG, HRP-linked $F(ab')_2$ fragment	GE Healthcare	NA9310
Amersham ECL Rabbit IgG, HRP-linked $F(ab')_2$ fragment	GE Healthcare	NA9340
Biological Samples		
Human adipose tissue specimens	The Alfred Hospital, Ethics No. 548-14	N/A
Chemicals		
Matrigel	Corning	FAL356230
BODIPY-493/503	ThermoFisher Scientific	D-3922
Collagenase, Type 2	Sigma Aldrich	C6885
ACK lysis buffer (RBC lysis)	ThermoFisher Scientific	A1049201
Transferrin	Sigma Aldrich	T8158
Biotin	Sigma Aldrich	B4639
Pantothenic acid	Sigma Aldrich	P5155
Human recombinant insulin	Actrapid, Nova Nordisk	1331415
Dexamethasone	Sigma Aldrich	D4902
Iso-butyl methyl xanthine	Sigma Aldrich	I5879
Rosiglitazone	Sigma Aldrich	R2408
Isoproterenol	Sigma Aldrich	I5627
Forskolin	Sigma Aldrich	F3917
Free glycerol reagent	Sigma Aldrich	F6428
Amplex Ultra Red	ThermoFisher Scientific	A36006
2-[1,2-3H(N)]-2DG	Perkin Elmer	NET549A001MC
Glucose D-[14C (U)]	Perkin Elmer	NEC042A001MC
Seahorse XF Base Medium	Seahorse Biosciences	SEA102353100
Seahorse XFe24 FluxPak 18 Assays	Seahorse Biosciences	SEA102340100
Critical Commercial Assays		
Ovation RNA-Seq system V2	NuGEN, San Carlos, USA	7102 (Protocol M01206v5, 2013)
Ovation Ultralow System V2	NuGEN, San Carlos, USA	0344 (Protocol M01379 v1, 2014)
Deposited Data		
Transcriptomics data	This paper	GSE129042

(*Continued on next page*)

Continued

REAGENT or RESOURCE	SOURCE	IDENTIFIER
Experimental Models: Organisms/Strains		
SCID mice (C.B-17/IcrHanHsd-Prkdcscid/ARC)	Animal Resources Centre, Australia	N/A
Oligonucleotides		
CEBPα	ThermoFisher Scientific	Hs00269972_s1
PPARγ	ThermoFisher Scientific	Hs00234592_m1
PLIN1	ThermoFisher Scientific	Hs00160173_m1
FABP4	ThermoFisher Scientific	Hs01086177_m1
TBP1	ThermoFisher Scientific	Hs99999910_m1
PPARGC1A	ThermoFisher Scientific	Hs01016719_m1
CITED1	ThermoFisher Scientific	Hs00918445_g1
TCF21	ThermoFisher Scientific	Hs00162646_m1
UCP1	ThermoFisher Scientific	Hs00222453_m1
Software and Algorithms		
Prism 7	GraphPad	https://www.graphpad.com
FlowJo	Tree Star	https://www.flowjo.com
Fiji	Schindelin et al., 2012	ImageJ
ClustVis	Metsalu and Vilo, 2015	https://biit.cs.ut.ee/clustvis/
STAR	Dobin et al., 2013	https://academic.oup.com/bioinformatics/article/29/1/15/272537
featureCounts	Liao et al., 2014	https://academic.oup.com/bioinformatics/article/30/7/923/232889
Voom	Law et al., 2014	https://genomebiology.biomedcentral.com/articles/10.1186/gb-2014-15-2-r29
fastQC tool		https://www.bioinformatics.babraham.ac.uk/projects/fastqc/

CONTACT FOR REAGENT AND RESOURCE SHARING

Further information and requests for resources and reagents should be directed to and will be fulfilled by the Lead Contact, Matthew Watt (matt.watt@unimelb.edu.au).

EXPERIMENTAL MODEL AND SUBJECT DETAILS

Human studies

Ethics approval was obtained from the Alfred Hospital Ethics Committee in accordance with the National Statement on Ethical Conduct in Human Research (2007) (Alfred Ethics Approval No. 548/14). All participants provided informed consent to participate in this study. Participants were undergoing various bariatric surgery procedures including laparoscopic banding, sleeve gastrectomy or open gastric bypass surgeries. The patient's full medical history was collected before surgery and fasting blood samples were taken prior to induction of anesthesia. Serum analysis was conducted at Alfred Pathology (Table S1).

Animal studies

Animal studies were approved by Monash Animal Research Ethics Committee, Monash University, Australia (Ethics Approval No. 089/2016). Male SCID mice were procured from Animal Resources Centre (Australia) and housed in the Animal Research Laboratory (ARL) facility (Monash University). Human APCs were transplanted in mice aged six weeks. Mice were fed a high fat diet for 12 weeks thereafter prior to tissue collection (42% calories from fat, Specialty Feeds).

METHOD DETAILS

White adipose tissue collection

Omental adipose tissue (VAT) was obtained from the distal portion of the greater omentum by laparoscopic techniques. ASAT was obtained by making an incision ~6 cm laterally from the umbilicus and GFAT was obtained from the upper lateral aspect of

the buttocks. Approximately 3-5 g of adipose tissue was excised from each depot of the patient. The excised tissues were immediately placed in tubes containing pre-gassed (95% O_2 / 5% CO_2), warm RPMI 1640 media with 1% bovine serum albumin (BSA), and 1% Penicillin-Streptomycin solution (Life Technologies) and transported to the analytical laboratory.

Isolation of the stromal vascular fraction and sorting of APCs

The adipose tissues obtained from VAT, ASAT and GFAT of each patient were processed separately, and the cells were isolated aseptically (sterile reagents, apparatus and tools) as described previously with minor modifications (Church et al., 2014; Lee and Fried, 2014). The tissues were rinsed twice in phosphate buffered saline (PBS), blot dried for 5 s and immediately placed in RPMI media (ThermoFisher Scientific Australia) containing 3% (w:v) BSA (Sigma Aldrich, Australia) and 1 mg/ml Type 2 Collagenase (Sigma Aldrich, Australia) at a ratio of 1:2 (g:ml). The tissues were minced into 5-10 mg pieces using scissors, transferred to a 37°C shaking water bath in 50 mL plastic tubes and incubated with agitation for 45 minutes. The digests were strained into fresh 50 mL plastic tubes using 210 μm nylon filters (SEFAR, Australia) to remove any undigested tissue and the tubes were spun at 1000 x *g* for 10 minutes at room temperature (RT). The floating mature adipocytes from each tube and the infranatants were discarded and the pellets containing the SVF cells were transferred to separate 1.7 mL plastic tubes in PBS (ThermoFisher Scientific, Australia) containing 0.02% EDTA (Sigma Aldrich, Australia) (PBS-EDTA) to restrict cell aggregation. The cells were spun and suspended in RBC lysis buffer (Life Technologies) for 5-10 minutes to lyse the RBCs. The resulting SVF cells from all three adipose tissue depots (in separate tubes) were further washed twice with PBS-EDTA at 4°C and once with ice-cold PBS-EDTA containing 2% BSA (FACS buffer). The cells were then suspended and blocked in ice-cold FACS buffer for two hours prior to antibody staining. From this step onward, the cells were placed on ice until sorted and cultured.

Antibody staining and FACS

The isolated and blocked SVF cells were strained through 40 μm filters to discard larger and aggregated cells, and resuspended in 1 mL of FACS buffer. The number of viable cells per ml per depot were counted using Trypan Blue solution (ThermoFisher Scientific Australia), which was also required to determine the antibody concentration required for staining. Thereafter, the antibody staining of single fluorochrome controls and sort samples was performed on ice for 15 min in the dark. The following antibody concentrations per $1x10^6$ cells were used: CD31 (1.5 μg), CD45 (0.5 μg), CD29 (0.5 μg) and CD34 (0.2 μg). Propidium iodide (PI) was added into the samples 5 min prior to the acquisition to distinguish the live and dead cells at the time of cell sorting.

The BD Influx FACS sorter (BD Biosciences) equipped with BD Sortware software (BD Biosciences) and four lasers was used for sorting the APCs at the FlowCore facility (Monash University). The laser alignment and drop delay using a 100 μm nozzle (pressure: 20 psi) was performed before sorting the cells as per the manufacturer instructions. Post adjustment for spectral compensation, three different APCs were identified based on their CD34 expression as $CD34^-$, $CD34^{lo}$ and $CD34^{hi}$ in each tissue depot. The identified APCs were then sorted into separate 1.7 mL tubes containing 200 μL of growth media consisting of α-minimal essential medium (α-MEM, ThermoFisher Scientific, Australia) containing 10% non-heat inactivated fetal bovine serum (FBS, ThermoFisher Scientific, Australia) and 1% penicillin-streptomycin (Pen-Strep) solution (ThermoFisher Scientific, Australia) at 4°C. The sorted cells were kept on ice until cultured. The data files generated during sample acquisition were processed using Flowjo software (Tree star, USA) to determine the frequencies for each gated cell population and FCS express software for t-SNE analysis (*De Novo* software, USA).

Histological analysis of human adipose tissue

Formalin fixed VAT, ASAT and GFAT were paraffin embedded and 10 μm sections were cut from each depot. The sections were hematoxylin-eosin stained. Briefly, the sections were deparaffinized in xylene, rehydrated in decreasing concentrations of ethanol, stained sequentially with hematoxylin and eosin and coverslipped with DPX mountant. The slides were imaged using a bright-field microscope (EVOS XL, ThermoFisher Scientific) and the acquired images were processed in Fiji (ImageJ) software equipped with Adiposoft plugin to measure adipocyte diameter. The minimum cell size was set to 40 μm and the average diameter was calculated for each depot. The total number of adipocytes was counted (per section) in patient-matched samples and the APC count for that patient was normalized to adipocyte number per section.

Transcriptomic profiling of APCs

The transcriptomes of the APC subtypes were assessed from the VAT of five patients (BMI 47.3 ± 1.4 (mean ± SEM) kg/m^2). The freshly sorted and uncultured APCs were washed twice using ice-cold DPBS at 1000 x *g* for 5 min and then spun at 12,000 x *g* for 10 min. The supernatant was discarded and the pellet was immediately frozen on dry ice for 30 min. Total RNA was extracted from the frozen samples by using RNeasy Mini kit (QIAGEN, Germany). Initially, the frozen pellets were thawed at room temperature for a minute and homogenized in 300 μL of RLT buffer containing 10% β-mercaptoethanol by passing through a 30 G (gauge) insulin syringe and the RNA was extracted as per manufacturer's instructions. The downstream sample processing and sequencing was performed at Monash Health Translation Precinct (MHTP, Clayton Australia) core facility. RNA quality of the samples was further assessed by measuring the RNA integrity number (RIN) using the Agilent 2100 Bioanalyzer (Agilent Biosystems) and the RNA concentration was assessed in a Qubit Bioanalyzer (ThermoFisher Scientific, Australia). The RNA samples were first amplified using the Ovation RNA-Seq system V2 kit (NuGEN, San Carlos, USA, protocol M01206v5, 2013) in a thermocycler and then subjected to

cDNA synthesis. Single Primer Isothermal strand-displacement Amplification (SPIA) technology was adopted to synthesize cDNA (Adiconis et al., 2013; Tariq et al., 2011). A total of 15 cDNA libraries were constructed from the RNA samples by this process.

The RNASeq libraries were then constructed from the cDNA samples by using the Ovation Ultralow System V2 (NuGEN, San Carlos, USA) as per the product instructions. Briefly, each cDNA sample was fragmented to generate blunt ends for the ligation of barcoded adaptor sequences. Each sample contained unique barcodes such that the samples were easily identified in the sequenced file. An equimolar pool (12 pM) of the all the ligated sample libraries, ~274 bp in size on an average, were pooled and hybridized onto two lanes of the HiSeq high-output flowcell per sample. The samples were sequenced in a Next Generation (Next Gen) HiSeq 1500 High Output platform (Illumina Inc, San Diego, USA protocol 15035788 rev D, Apr 2014) by following 50 bp single-end Short Read (SR) sequencing chemistry, resulting in ~19 million reads per library. Fastq files (containing the sequence reads) and fastQC files (containing Quality Control information about the starting material used and sequencing) were generated for each library to assist with the sequence analysis. During analysis, the adaptor sequences were removed from the 50 bp short reads and the low quality reads toward the 3′ end was trimmed (Conesa et al., 2016). The trimmed reads were further assessed using the fastQC tool to select the high quality reads. The quality passed sequences were then mapped to the human genome (version hg19, downloaded from Ensembl) using the Spliced Transcripts Alignment to a Reference (STAR) software (Dobin et al., 2013). Uniquely mapping read-pairs were assigned to annotated transcript exons (including splice-junctions) contained in the Ensembl GTF (General Transfer Format) file for genome build hg19 using FeatureCounts (Liao et al., 2014), aggregating at the gene level to produce gene-wise counts for each sample. Genes that failed to accrue at least one count-per-million reads (cpm) in at least three samples were filtered out and the samples were normalized for library size by the TMM (trimmed mean of M vales) method (Robinson and Oshlack, 2010).

The mapped read counts were further subjected to variance-stabilizing (VST) normalization to minimize the coefficient of variation in the expression of genes between the APC subtypes (Bullard et al., 2010; Zwiener et al., 2014). To understand the closeness between the APC subtypes, the Euclidean distance between the normalized mapped annotated reads (genes) was calculated followed by hierarchical clustering of the samples. Additionally, principal component analysis (PCA) was conducted to validate the hierarchical clustering of APC subtypes. The annotated genes were then tested for differential gene expression between the APC subtypes by using the voom function (Law et al., 2014) and the $\log_2$ values of the counts were calculated to facilitate the linear modeling of the data. The differential gene expression (log fold changes - Log FC) and the significance between the $CD34^{hi}$ versus $CD34^{lo}$, $CD34^{hi}$ versus $CD34^{-}$, and $CD34^{lo}$ versus $CD34^{-}$ APC groups was then determined by Limma, an "R" package (Bioconductor). Considering the high number of genes identified, the p values between the APC subtypes for each gene were subjected to false discovery rate (FDR) measurements to calculate the adjusted p values (adj. p value) by following Benjamini-Hochberg procedure.

The differential gene expression results (FDR < 0.05 and log fold change (FC) > 1) between $CD34^{hi}$ versus $CD34^{lo}$, $CD34^{hi}$ versus $CD34^{-}$, and $CD34^{lo}$ versus $CD34^{-}$ APC subtype groups was subjected to Ingenuity Pathway Analysis (IPA, QIAGEN Bioinformatics). The top canonical pathways predicted to modulate the signaling and metabolic functions by the differentially expressed genes between the APC groups were identified. The significance of the predicted functions was determined based upon the "activation z-scores."

Culturing of sorted APCs

The sorted cells were washed in the growth media once at 1000 g for 5 min at 4°C and then cultured in T-25 flasks (Corning, Australia) containing 5 mL of growth media at 37°C in a carbon dioxide (CO_2) (5%) incubator (ThermoFisher Scientific, Australia). The media was replenished every 3 or 4 days until the cells reached confluence (Passage – P0), after which the cells were detached with 1 mL of 0.05% Trypsin-EDTA solution (Sigma Aldrich, Australia) at 37°C for 5 min and neutralized with growth media. The cells were collected in 15 mL plastic tubes and spun at 1000 x *g* for 5 min at 4°C. The pellets were suspended in the growth media and were used for experiments.

Assessment of cell proliferation

Passage 2 APCs ($CD34^{hi}$, $CD34^{lo}$ and $CD34^{-}$) were cultured in 24-well plates (10,000 cells per well) with 500 μL of growth medium per well at 37°C in a CO_2 (5%) incubator and the number of cells were counted on day 1, 2, 4 and 6 of incubation. Briefly, on the specified days, cells were gently washed with 500 μL of DPBS, detached using 80 μL of 0.05% Trypsin-EDTA solution at 37°C for 5 min, neutralized with 300 μL of growth media and collected in 1.7 mL tubes. The wells were washed once more with 700 μL of DPBS and then collected in to corresponding tubes containing the trypsinized cells. The tubes were spun at 1,000 x *g* for 5 min at 4°C and the cell pellets were resuspended in 50 μL of cold DPBS. Approximately 10 μL of the cell suspension was loaded into a hemocytometer and the cells were counted under a microscope (10X magnification, EVOS XL, ThermoFisher Scientific, Australia).

Adipogenic differentiation

Prior to differentiation, the P1 cells were cultured to confluence in triplicate for each experiment in 12-well plates with 1 mL of growth media at 37°C in a CO_2 (5%) incubator. After reaching confluence, the monolayer of cells was gently washed twice with sterile DPBS and were incubated in differentiation basal media consisting of DMEM F-12, 1% Pen-Strep, 200 pM T3 (Sigma Aldrich, Australia), 10 μg/ml transferrin (Sigma Aldrich, Australia), 3.3 μM biotin (Sigma Aldrich, Australia), and 17 μM pantothenic acid (Sigma Aldrich, Australia). During the first three days of differentiation, the media was supplemented with 20 nM human recombinant insulin (Actrapid®, Nova Nordisk, Australia), 250 nM dexamethasone (Sigma Aldrich, Australia), 500 μM Iso-butyl methyl xanthine (IBMX, Sigma Aldrich, Australia) and 2 μM rosiglitazone (Sigma Aldrich, Australia). Rosiglitazone was withdrawn after 3 days and IBMX was withdrawn after 7 days. The differentiated APCs (adipocytes) were maintained in basal media containing 20 nM insulin and

250 nM dexamethasone, which was replenished every 3 days until assayed. For cellular metabolic assessments, the differentiated APCs were hormone starved for 2 days on day 11 of differentiation prior to experimentation.

Xenotransplantation of APCs

APCs ($\sim 10^6$ cells/subtype) were freshly sorted from the SVF isolated from ~15 g of ASAT of four individual patients in a BD FACSAria III (BD Biosciences) cell sorter using BD FACSDiva software (BD Biosciences) at the Melbourne Brain Centre flowcytometry facility (The University of Melbourne) as described above. The sorted cells were suspended in 50 μL of Matrigel (Corning, Australia) per subtype per subject. Six week old male SCID mice were anaesthetised using isoflurane prior to the cell injections. The dorsal side of each mouse was swabbed with 70% ethanol and the APCs suspended in Matrigel ($\sim 10^6$ cells / per mouse) were injected using a 29G gauge syringe into the right side of the dorsal flank. Only one APC subtype was injected per mouse. The left side of the dorsal flank of each mouse was injected with 50 μL of Matrigel alone to serve as a control. Post recovery, the mice were fed a high fat diet (Specialty Feeds, Australia) and killed at twelve weeks by cervical dislocation to obtain the grafted tissues for imaging purposes. Epididymal adipose tissue (mouse endogenous adipose tissue) and Matrigel were also harvested.

Whole-mount imaging of the graft

The harvested xenografts from each cohort (three mice per subject), mouse adipose tissue and Matrigel samples were subjected to whole-mount imaging on the same day of the cull as previously prescribed (Berry et al., 2014a). Briefly, the tissues were minced into ~4 mm^3 pieces and fixed in 1% paraformaldehyde for 15 min at room temperature. The fixed tissues were rehydrated in DPBS 3 × 10 min each and stained with BODIPY-493/503 (ThermoFisher Scientific, Australia) (2 μg/ml to visualize the mature adipocytes), DAPI (ThermoFisher Scientific, Australia) (1 μg/ml, to visualize the nuclei) and anti-human CD29 antibody (1:25, to locate the human cells) (Biolegend, USA) (Xu et al., 2015) for 30 min on ice in the dark. The stained tissues were washed 3 × 10 min with DPBS to remove any unbound dyes and antibody. The tissues were then placed on microscope slides within boundaries marked by Vaseline and mounted with FluoromountG (ThermoFisher Sceintific, Australia). The slides were imaged in a Leica SP5 inverted confocal microscope (Leica Microsystems, Mannheim, Germany) at the Biological Optical Microscopy Facility (The University of Melbourne) using the 20X dry long-working distance objective. As the cells were distributed within a 3D landscape of the whole-mount, the exposure settings for each fluorochrome was adjusted to minimize signal saturation. The control tissues (mouse epididymal adipose tissue and Matrigel) were imaged using equivalent exposure settings used at the time of analysis. The acquired images were processed in Fiji (ImageJ) software.

Immunohistochemistry of the graft

The xenograft was formalin fixed (10%) overnight at 4°C. After fixation, the tissue was transferred to 70% ethanol, then paraffin embedded, sectioned and stained with CD29, PLIN1 and DAPI. The sections were deparaffined in xylene (4 min) and rehydrated using decreasing concentrations of ethanol and finally run under tap water for 2 min. The sections then underwent antigen retrieval by being immersed in 10 mM sodium citrate + 0.05% Tween-20, pH 6.0 at 95°C for 15 min. The sections were then thoroughly washed with 0.1M PB and endogenous peroxidase activity was blocked using 1% H_2O_2 in 0.1 M PB for 15 min and washed again. The sections were then further blocked using 4% Normal Goat Serum and 0.3% Triton X-100 in 0.1M PB for 2 h. An additional universal blocking agent (CAS block; Invitrogen, #008120) was used for 10 min to minimize background staining. The sections were then incubated with the primary antibodies CD29 (1:25, BioLegend, #303018) and Perilipin 1 (1:1000, Abcam, #ab61682) for 24 h at 4°C Sections were covered to minimize light exposure. Following the primary antibody incubation, the sections were washed thoroughly with 0.1 M PB and incubated with AlexaFluor 488 Donkey-anti Goat secondary antibody (1:400, Invitrogen, #A11055) for 90 min at room temperature. After thoroughly washing the sections they were mounted using antifade mounting media containing DAPI (Vectashield, #H-1500). The slides were imaged using a Zeiss Axio Imager M2.

Gene expression analysis

Total cellular RNA was extracted by using PureLink® RNA Mini Kit (ThermoFisher Scientific, Australia). Briefly, 300 μL of lysis buffer containing 10% β-mercaptoethanol was added to the wells and the cells were lifted with plastic cell scrapers (TRP, Australia). The cells were further homogenized by passing through an insulin syringe (BD, Australia). The RNA was then isolated as per manufacturer's instructions. The RNA concentration and quality of all samples was measured in a Nanodrop ND-1000 spectrophotometer (ThermoFisher Scientific, MA, USA). The RNA was reverse-transcribed using the iScript cDNA synthesis kit (Biorad, Hercules, CA). The mRNA content was then assessed by quantitative PCR (qPCR) using the AmpliTaq Gold fast PCR master mix kit (ThermoFisher Scientific) in a Realplex Mastercycler (Eppendorf, Germany). The primer / probe mixes were purchased from Applied Biosystems and the mRNA levels of *TBP1* was used to normalize the gene expression data.

Immunofluorescence microscopy

The P1 APCs were cultured in chambered coverslips (Sarstedt, Germany). On day 12 of differentiation, the media was removed and the cells were fixed in 4% paraformaldehyde for 15 min at RT, rehydrated in DPBS (3 × 5 min washes). The fixed cells were blocked and permeabilized in DPBS containing 1% BSA and 0.01% saponin (Sigma Aldrich, Australia) (permeabilization buffer) for 30 min at RT. The antibody solutions were prepared in the permeabilization buffer. The cells were then stained with the anti-PLIN1 primary

antibody overnight at 4°C in a humidified chamber. The next day, cells were washed 3 × 5 min with DPBS containing 1% BSA (IF wash buffer) and then incubated with a donkey anti-goat secondary antibody for 60 min at RT in a humidified chamber, protected from light. The secondary antibody was prepared in the IF permeabilization buffer along with DAPI (ThermoFisher Scientific, Australia) (1 μg/ml, to visualize the nuclei) and BODIPY-493/503 (ThermoFisher Scientific, Australia) (1 μg/ml to visualize the lipid droplets). The wells were then washed 3 × 5 min with DPBS containing 1% BSA (IF wash buffer) and added with a mounting media containing 5% glycerol then imaged using a Leica SP8 inverted confocal microscope (Leica Microsystems, Mannheim, Germany) at the Monash Micro Imaging facility using 63X objective (oil-immersion). The acquired images were processed in Fiji (ImageJ) software.

Immunoblot analysis

The differentiated APCs (day 13) were homogenized in RIPA buffer and solubilized lysates were resolved by SDS-PAGE. The separated proteins were transferred to PVDF membranes to probe for ATGL, HSL, GO-S2, CGI-58 and PLIN1. The details of the primary and secondary antibodies used for blotting are mentioned in the Key Resources Table.

Metabolic assessments

Lipolysis

The medium was removed from the hormone starved differentiated APCs on day 13, the cells were washed twice with warm DPBS and incubated in 300 μL of lipolysis basal media, which consisted of phenol-red free low glucose (LG, 5 mM) Dulbecco's Minimal Essential medium (DMEM) containing 2% fatty acid free BSA (Bovogen, Australia). Stimulated lipolysis was assessed in the same lipolysis medium with the addition of 1 μM isoproterenol (pan β-adrenergic activator) or 20 nM forskolin (adenylate cyclase activator, increases cyclic-adenosine monophosphate (cAMP) and protein kinase A (PKA) activity). Cells were incubated for 4 h at 37°C. At the end of the experiment, the media was collected and frozen at −20°C. The amount of glycerol released in the media was later quantified using an enzymatic colorimetric assay as described previously (Clark et al., 2009). The fluorescence was measured in a fluorimeter (Clariostar, BMG LABTECH, GmbH, Germany Ex: 490 nm / Em: 590 nm) and the glycerol concentration was processed using MARS Data Analysis (powered by MATLAB).

Measurement of fatty acid metabolism

On day 13 of differentiation, the hormone starvation media was removed from the cells and were washed twice with warm DPBS and incubated with 500 μL of DMEM-LG media containing 2% BSA, 0.5 mM oleic acid and 0.5 μCi/ml of [1-^{14}C]-oleic acid (PerkinElmer, MA, USA) for 4 h at 37°C. Complete fatty acid oxidation was assessed by collecting the $^{14}CO_2$ released from the acidified media (in 1M NaOH), to which 4 mL of scintillation fluid was added (Ultima Gold, Perkin Elmer, USA) and radioactivity determined by scintillation counting (LS 6500 Beckman Coulter, USA). Incomplete oxidation (the acid-soluble metabolites, ASMs) were also assessed. The cells were washed three times with 1 mL of ice-cold DPBS, frozen then lysed in ice-cold DPBS containing 0.1% Triton X-100. An aliquot was used for total protein measurements using the Pierce BCA assay (ThermoFisher Scientific Australia). The lipids in the remaining cells were extracted with 900 μL of 2:1 v/v chloroform: methanol solution, sealed and incubated at room temperature for 2 h. The tubes were mixed every 10 min during the incubation. After 2 h, the tubes were spun at 1000 x *g* for 10 min at 4°C to separate the aqueous and organic phases. The upper aqueous layer was collected and transferred to scintillation tubes for assessment of radioactivity. Total fatty acid oxidation was calculated by summing the $^{14}CO_2$ and ^{14}C-ASMs.

The organic phase containing the lipids was collected into fresh 12 × 75 mm glass tubes and was evaporated to dryness under a stream of nitrogen at 40°C. The dried samples were then dissolved in 2:1 v/v chloroform: methanol solution containing a small amount of glycerol tripalmitate (triglyceride standard) using a Hamilton syringe. The samples were applied to the corresponding glass backed thin layer chromatography plate (Silica Gel 60, Analtech, DE, USA) and resolved in 60:40:3 v/v heptane: isopropyl ether: acetic acid. Triglyceride bands were visualized under UV light and scraped into scintillation tubes. The rest of the sample from the solvent front to approximately 2 cm from the sample loading point were also scraped into separate scintillation tubes to measure incorporation of fatty acids into lipids other than triglyceride. The scintillation tubes were filled with 2 mL of scintillation fluid and the radioactivity was determined. The total fatty acid uptake was determined by adding the of fatty acid oxidation, triglyceride esterification and esterification into other lipids.

Measurement of glucose uptake

Glucose uptake was measured by a radiometric method. Briefly, the medium from the insulin-starved cells was removed and the cells were washed twice with DPBS. The cells were pre-incubated in 10 μM 2-deoxy-D-glucose (2-DG) in DMEM containing 0.1% BSA (Bovogen, Australia) for 10 min at 37°C. The pre-incubation medium was replaced with the same medium but with the addition of 1 μCi/ml of 2-[1,2-^{3}H(N)]-2DG (^{3}H-2DG, PerkinElmer, MA, USA). The cells were incubated at 37°C for 10 min and the media was immediately removed. The cells were washed three times with ice-cold DPBS then lysed in ice-cold DPBS containing 0.1% Triton X-100. The cells were further mechanically disrupted five times with a 0.3 mL insulin syringe (BD, Australia). An aliquot was used for total protein measurements using the Pierce BCA assay (ThermoFisher Scientific Australia). The remaining cell lysate was added to scintillation tubes filled with 2 mL of scintillation fluid (Ultima Gold, Perkin Elmer, USA) and the radioactivity was determined (LS 6500 Beckman Coulter, USA).

Measurement of mitochondrial respiration

Uncoupling respiration or thermogenic potential of the differentiated APCs was measured in the ASAT (n = 4) derived differentiated APCs in a Seahorse XF^{e}24 Extracellular Flux Analyzer (Seahorse Bioscience). The cells were grown in Seahorse XF24 plates, differentiated, and at day 13 hormone starved as described previously. Seahorse XF^e basal media (pH 7.4) containing 2.5 mM glucose, 2 mM glutamine, 1 mM sodium pyruvate was added. The plates were then in a 37°C for 30 min in the absence of CO_2. The oxygen consumption rate (OCR) was measured three times at 8 min intervals at baseline and three times subsequently after the addition of oligomycin (5 μM, Complex V / ATP synthase blocker), five times after the addition of either basal media (vehicle / control) or basal media containing Isoproterenol (1 μM, pan β-adrenergic activator), three times after the addition of FCCP (3 μM) and three times after Antimycin A (5 μM, Complex III blocker) + Rotenone (5 μM, Complex I blocker) injection. Data were normalized for protein concentration as described above. The last measurement (of the three measurements) from the baseline readings, lowest reading post oligomycin treatment, three highest values after vehicle / isoproterenol treatment, highest value post FCCP injection and the lowest value post Antimycin A + Rotenone injection per cell type per subject were used for calculations. The non-mitochondrial respiration was then excluded from the baseline. Proton leak is reported as the difference between the oligomycin treatment and non-mitochondrial respiration. All the reported values were normalized to their corresponding control values (vehicle versus isoproterenol samples).

Secretome analysis

The differentiated APCs (day 13) were incubated with 10 mL of EX-CELL® protein-free CHO serum-free medium for 24 h. The medium was collected and centrifuged at 300 x *g* for 10 min at 4°C. The supernatant containing the secreted proteins was collected and stored at −80°C. The cell monolayer was washed with ice-cold DPBS and lysed to assess total protein content. The samples for LC/MS analysis were prepared at Monash Biomedical Proteomics Facility (MBPF, Victoria, Australia). The cellular protein content of all the differentiated APC subtypes was normalized and an appropriate volume of conditioned media from each sample was buffer exchanged and concentrated in Amicon Ultra-4 centrifugal filters pre-hydrated with Tris (50 mM, pH 8) sodium chloride (150 mM) buffer at 4000 x *g* for 45 min. The protein content of the concentrated samples was determined. After reducing the disulphide bonds using Tris(2-carboxyethyl)phosphine hydrochloride (TCEP, final concentration 10 mM) at 65°C for 20 min, the samples were subjected to an in-house modified Filter-Aided Sample Preparation (FASP) protocol. In brief, the samples were diluted in a 4% Sodium Dodecyl Sulfate (SDS) buffer (pH: 8.1) containing DTT (100mM), Tris-HCL (100 mM) and transferred to a 10 kDa spin cartridge containing an Omega membrane (Pall). The SDS from the denatured proteins was removed by adding Tris HCL buffer (pH: 8.1) containing 8 M urea (urea solution). The process was repeated once again and the samples on the cartridge were alkylated with chloroacetamide (100 mM) and urea solution in the dark. The samples were washed three times using urea solution and desalted twice with triethylammonium bicarbonate solution (TEAB, Sigma). The spin cartridge was inserted into a new tube and the samples were treated with Trypsin solution (1:100) overnight at 37°C. The next day, trypsinized samples were centrifuged twice with 100 mM TEAB solution at 14,000 x *g* for 10 min each without discarding the flow through and the digested peptides were finally eluted with 0.5 M sodium chloride solution at 14,000 x *g* for 10 min. The peptides were acidified with 2% formic acid to deactivate the trypsin, desalted and purified using Zip tips packed with C18 reversed phase resin (Agilent Technologies) and eluted in 50% acetonitrile and 0.1% formic acid. The eluted samples were dehydrated and resuspended in 0.1% formic acid containing iRT (indexed retention time (Escher et al., 2012)) peptides.

The peptides were loaded onto an Acclaim PepMap RSLC analytical column (75 μm (inner diameter) x 50 cm (length) equipped with a nanoViper C18, 2 μm (particle size), 100Å (pore size); Thermo Scientific) using an Acclaim PepMap 100 trap column (100 μm (inner diameter) × 2 cm (length), nanoViper, C18, 5 μm (particle size), 100 Å (pore size); Thermo Scientific). The peptides were then separated on a Dionex UltiMate 3000 RSLCnano Liquid Chromatography (LC) system (Thermo Scientific) and analyzed in a quadrupole Orbitrap mass spectrometer, Q Exactive Plus™ (Thermo Scientific) using a data-dependent acquisition (DDA) approach. The acquired raw data files were analyzed with MaxQuant (v.1.6.0.16) in combination with the human Swissprot database to identify and quantify all the proteins across the various APC subtypes with a false discovery rate (FDR) of 1%. The normalized data was statistically analyzed using Perseus (v1.6.0.7) software to determine the differentially expressed (Log_2 FC > 1.5, $p < 0.05$) proteins using a two-sided Student's t test. Heatmaps and principle component analysis of the differentially expressed proteins was performed using the software clustVis. The data was subjected to IPA analysis as described above.

QUANTIFICATION AND STATISTICAL ANALYSIS

Statistical analysis was performed using one-way or two-way analysis of variance (ANOVA) with repeated-measures, where appropriate, and specific differences were located using a Bonferroni post hoc test. Paired or unpaired Student's t tests were used for some analysis as described in the Figure legends. Where the data was not normally distributed, as determined by Shapiro-Wilk normality test, non-parametric testing was conducting using a Friedman test with Dunn's multiple comparison. Statistical significance was set *a priori* at $p \leq 0.05$. Data are expressed as means ± SEM.

DATA AND SOFTWARE AVAILABILITY

The accession number for the RNA-Seq data of the 15 APC cell types is GEO: GSE129042